Neurobiology of Disease 158 (2021) 105469

Contents lists available at ScienceDirect

Neurobiology of Disease

journal homepage: www.elsevier.com/locate/ynbdi

Glial contribution to cyclodextrin-mediated reversal of cholesterol accumulation in murine NPC1-deficient neurons *in vivo*

Amélie Barthelemy [a,1], Valérie Demais [b,1], Izabela-Cristina Stancu [c], Eugeniu Vasile [d], Tom Houben [a,1,2], Michael Reber [a,3], Valentina Pallottini [e,f], Martine Perraut [a], Sophie Reibel [g], Frank W. Pfrieger [a,b,*]

[a] Centre National de la Recherche Scientifique, Université de Strasbourg, Institut des Neurosciences Cellulaires et Intégratives, Strasbourg, France
[b] Plateforme Imagerie in Vitro, CNRS UPS 3156, Neuropôle, 8 allée général Rouvillois, 67084 Strasbourg, France
[c] Advanced Polymer Materials Group, Faculty of Applied Chemistry and Material Science, University Politehnica of Bucharest, 1-7 Gh. Polizu Street, 011061 Bucharest, Romania
[d] Faculty of Applied Chemistry and Materials Science, Department of Science and Engineering of Oxide Materials and Nanomaterials, University Politehnica of Bucharest, 1-7 Gh. Polizu Street, 011061 Bucharest, Romania
[e] Dept. Science, Biomedical and Biotechnology Section, University Roma Tre, 00146 Rome, Italy
[f] Neuroendocrinology, Metabolism and Neuropharmacology Unit, IRCSS Fondazione Santa Lucia, Via del Fosso Fiorano 64, 00143 Rome, Italy
[g] Chronobiotron UMS 3415, Université de Strasbourg, 8 allée général Rouvillois, 67084 Strasbourg, France

ARTICLE INFO

Keywords:
Lysosome
Intravitreal
Cyclodextrin
Inherited metabolic disease
Ganglion cells
Amacrine cells
Microglia
Astrocytes
Müller cells
Neutrophil granulocytes

ABSTRACT

Niemann-Pick type C disease is a rare and fatal lysosomal storage disorder presenting severe neurovisceral symptoms. Disease-causing mutations in genes encoding either *NPC1* or *NPC2* protein provoke accumulation of cholesterol and other lipids in specific structures of the endosomal-lysosomal system and degeneration of specific cells, notably neurons in the central nervous system (CNS). 2-hydroxypropyl-beta-cyclodextrin (CD) emerged as potential therapeutic approach based on animal studies and clinical data, but the mechanism of action in neurons has remained unclear. To address this topic *in vivo*, we took advantage of the retina as highly accessible part of the CNS and intravitreal injections as mode of drug administration. Coupling CD to gold nanoparticles allowed us to trace its intracellular location. We report that CD enters the endosomal-lysosomal system of neurons *in vivo* and enables the release of lipid-laden lamellar inclusions, which are then removed from the extracellular space by specific types of glial cells. Our data suggest that CD induces a concerted action of neurons and glial cells to restore lipid homeostasis in the central nervous system.

1. Introduction

Niemann-Pick type C (NPC) disease (OMIM #257220, OMIM #607625) is a rare, autosomal recessive and ultimately fatal lysosomal storage disorder with variable disease onset, multiple visceral and neurologic symptoms and diverging life spans (Bräuer et al., 2019; Gowrishankar et al., 2020; Hammond et al., 2019; Vanier, 2010; Wheeler and Sillence, 2020). The disease is caused by mutations in *Npc1* (Loftus et al., 1997) or *Npc2* (Naureckiene et al., 2000) that encode a membrane-resident and an intralumenal component of the endosomal-

Abbreviations: ACL, amacrine cell layer; B/M, bipolar cells and Müller cells; BSA, bovine serum albumin; CD, 2-hydroxypropyl-beta-cyclodextrin; CDAuNPs, CD-gold nanoparticles; CNS, central nervous system; GCL, ganglion cell layer; GCM, glia-conditioned medium; HOR, horizontal cells; IPL, inner plexiform layer; NP mouse, NPC1-deficient mouse; NPC, Niemann-Pick type C; ONL, outer nuclear layer; OPL, outer plexiform layer; PBS, phosphate-buffered saline; RGCs, retinal ganglion cells; RT, room temperature; TEM, transmission electron microscopy; U18666A, 3-β-[2-(diethylamine)ethoxy]androst-5-en-17-one; WT, wild-type.

* Corresponding author at: INCI CNRS UPR 3212, 8 allée général Rouvillois, 67084 Strasbourg, France.
E-mail address: frank.pfrieger@unistra.fr (F.W. Pfrieger).

[1] These authors contributed equally.

[2] Present address: Dept. Genetics and Cell Biology, School of Nutrition and Translation Research in Metabolism (NUTRIM), Maastricht University, 6229 ER Maastricht, The Netherlands.

[3] Present address: Krembil Research Institute, University Health Network – Dept. Ophthalomology and Vision Sciences, University of Toronto, 60 Leonard Av., Toronto, ON M5T 0S8, Canada.

https://doi.org/10.1016/j.nbd.2021.105469
Received 8 April 2021; Received in revised form 17 July 2021; Accepted 2 August 2021
Available online 5 August 2021

lysosomal system, respectively (Kwon et al., 2009; Li et al., 2017; Pfeffer, 2019; Qian et al., 2020; Winkler et al., 2019). Dysfunction of either protein causes accumulation of unesterified cholesterol and other molecules in late endosomes-lysosomes (Breiden and Sandhoff, 2020; Demais et al., 2016; Kobayashi et al., 1999; Liscum et al., 1989; Lloyd-Evans et al., 2008; Reid et al., 2004; Sokol et al., 1988; Zervas et al., 2001). The pathologic accumulation of cholesterol can be visualized by light microscopy following cyto- or histochemical staining with filipin (Pentchev et al., 1985), a bacteria-derived fluorescent polyene that binds unesterified cholesterol (Norman et al., 1972). Filipin staining of patient-derived fibroblasts has served as diagnostic test for the disease (Vanier and Latour, 2015). Electron microscopy revealed the presence of inclusions filled with membranes in neurons of NPC disease patients (Anzil, 1973; Harzer et al., 1978; Love et al., 1995; Palmer et al., 1985) and of animal models (Claudepierre et al., 2010; Davidson et al., 2009; German et al., 2002; Lowenthal et al., 1990; Phillips et al., 2008; Praggastis et al., 2015; Tanaka et al., 1988). These structures probably represent the ultrastructural correlate of lipid accumulation (Demais et al., 2016; Kwiatkowska et al., 2014).

At present, therapeutic options for NPC disease are limited, notably with respect to progressive neurologic symptoms (Geberhiwot et al., 2018; Toledano-Zaragoza and Ledesma, 2020). Several genetic and pharmacologic approaches are currently under study (Pallottini and Pfrieger, 2020). Cyclodextrins emerged as potential therapeutic approach based on a surprising finding: beneficial effects in NPC1-deficient (NP) mice originally attributed to allopregnanolone (Griffin et al., 2004) were in fact induced by CD serving as vehicle (Davidson et al., 2009; Liu et al., 2008; Liu et al., 2009). Cyclodextrins are naturally occurring, water-soluble cyclic oligosaccharides with a cone-like shape that bind-and thereby solubilize-hydrophobic molecules (Coisne et al., 2016; Crini, 2014; Kurkov and Loftsson, 2013). Due to their size and the absence of a specific natural transport system, cyclodextrins hardly cross the intact blood-brain barrier (Banks et al., 2019; Camargo et al., 2001; Monnaert et al., 2004; Pontikis et al., 2013). Direct delivery of CD into the brain slowed neurologic disease progression in mouse and cat models (Pallottini and Pfrieger, 2020) of the disease (Aqul et al., 2011; Vite et al., 2015) and in human patients (Berry-Kravis et al., 2018; Farmer et al., 2019; Ory et al., 2017).

At present, it is unclear how CD accomplishes its beneficial effects in NPC disease *in vivo*. Previous studies investigated how CD affected animal models and patients after chronic administration for weeks to months (Aqul et al., 2011; Berry-Kravis et al., 2018; Farmer et al., 2019; Fukaura et al., 2021; Ory et al., 2017; Palladino et al., 2015; Praggastis et al., 2015; Vite et al., 2015), but the immediate effects of CD on brain cells remain unknown despite growing interest in CD-based therapies for other neurodegenerative diseases (Coisne et al., 2016). Here, we addressed this fundamental question using the retina as accessible part of the CNS that is affected by NPC1 dysfunction in humans (Havla et al., 2020; Palmer et al., 1985) and in animal models (Claudepierre et al., 2010; Palladino et al., 2015; Phillips et al., 2008; Yan et al., 2014a). For drug administration, we chose intravitreal injections that enable direct delivery of molecules to the retina and subsequent monitoring of drug effects at defined time points (Del Amo et al., 2017). Vehicle injections in the contralateral eye establish the control condition in the same animal. To locate CD inside cells we coupled the compound to gold nanoparticles, which can be visualized by transmission electron microscopy (TEM).

2. Material and methods

2.1. Animals

Experimental procedures involving animals and their care were performed in accordance with European and French regulations on the protection of animals used for scientific purposes (EU Directive 2010/63/EU and its transposition into the French regulation 2013–118, project authorised by the French Ministry of Research after ethical evaluation APAFIS#2016021212596886). All experiments were performed with 4-weeks-old Balb/c mice homozygous for the recessive NIH allele of *Npc1* (NP mice) or wild-type (WT) littermates (BALB/cNctr-Npc1^{m1N}/J; Stock 003092; The Jackson Laboratory; Chronobiotron, UMS 3415, Strasbourg, France, >30 generations of in-house matings). Since we studied immediate effects of CD on retinal neurons, presymptomatic mice were used to reduce suffering. Mice were housed under specific-pathogen-free standard operating procedures (NP mouse colony positive for *Helicobacter sp*, *Rodentibacter sp* and mouse norovirus) in an individually ventilated caging system and at the following environmental conditions: 12/12 h light/dark cycle (lights on at 7 am), temperature 21.5–23 °C, 40–50% relative humidity. Autoclaved aspen wood chips (SAFE Lignocell Select) and nesting material (cotton squares and aspen chewing bars) were used as bedding environmental enrichment. Sterile-filtered or autoclaved tap water and irradiated standard rodent chow (SAFE A03–10, A04–10) were available *ad libitum*. Mice were genotyped as described (Buard and Pfrieger, 2014). Animals of either sex were used.

2.2. Production and validation of CD-coupled gold nanoparticles

CD-gold nanoparticles (CDAuNPs) were prepared by fast reduction of the gold precursor chloroauric acid with sodium borohydride in the presence of CD. Using this method, cyclodextrin stabilizes nascent gold nanoparticles through hydrophobic-hydrophobic interactions without changing its binding properties (Cutrone et al., 2017; Liu et al., 2003). Briefly, a solution containing 10 mM CD in 0.25 mM $HAuCl_4$ [50 mL; Au (III) chloride hydrate, Sigma–Aldrich, Steinheim, Germany) was prepared in double distilled water (GFL bidistiller apparatus). Then, 100 μL aliquots of freshly prepared 0.1 M sodium borohydride ($NaBH_4$) were added, at room temperature (RT; 20–24 °C), until a stable orange colloid was noticed (1.2 mL of $NaBH_4$). The reaction was allowed to proceed for 24 h at RT. Resulting colloidal solutions were filtered using 0.45 μm Millipore filters, and stored at 4 °C. CDAuNPs were deposited on a TEM copper grid covered with a thin amorphous carbon film with holes. High resolution TEM analyses of the film structure were performed using a TECNAI F30 G2 S-TWIN microscope operated at 300 kV and equipped with detectors for energy-dispersive X-ray and electron energy loss spectrometry.

Effects of CDAuNPs on cholesterol accumulation were examined using serum-free primary cultures of retinal ganglion cells (RGCs). RGCs were purified from 1-week-old Wistar HAN rats (Chronobiotron, UMS 3415, Strasbourg, France) and cultured as described (Demais et al., 2016). Briefly, retinae were dissected and subjected to mechanic and enzymatic dissociation (Neural Tissue Dissociation Kit - Postnatal Neurons, Miltenyi Biotec). RGCs were purified using a subtraction (primary: rabbit anti-rat macrophage, Axell/Wak Chemie AI-A51240; secondary: goat anti-rabbit IgG, Jackson ImmunoResearch 111–005-003) and a

selection step (primary: anti rat Thy1.1/CD90 clone T11D7e; secondary: goat anti-mouse IgM, Jackson ImmunoResearch 115–005-003) and plated on poly-D-lysine-coated 96-well microplates (7000 cells per well; black/clear imaging plate, BD Falcon 353,219). RGCs were cultured in serum-free medium (Neurobasal/Invitrogen) supplemented with MACS Neurobrew-21 (Miltenyi Biotec), brain-derived neurotrophic factor (25 ng/mL; PeproTech, London, UK), ciliary neurotrophic factor (10 ng/mL; PeproTech), forskolin (10 μM; Sigma), glutamine (2 mM; Invitrogen), *N*-acetylcysteine (60 μg/mL; Sigma), penicillin (100 units/mL; Invitrogen), sodium pyruvate (1 mM; Invitrogen), streptomycin (100 μg/mL; Invitrogen). RGCs were treated with glia-conditioned medium (GCM) after one day in culture. GCM was prepared as described (Nieweg et al., 2009). Briefly, mechanically dissociated cortices from one- to three-days-old Wistar rats were cultured in poly-D-lysine-coated (10 μg/mL; Sigma P7886) tissue culture plates (diameter 10 cm, BD Falcon Cat. 353,003) in DMEM (#21969), heat-inactivated fetal calf serum (10%), penicillin (100 units/mL), streptomycin (100 μg/mL) and glutamine (2 mM) (all Gibco/Invitrogen). After 2 weeks, culture plates were washed with phosphate-buffered saline (PBS) and glial cells were cultured in Neurobasal supplemented with glutamine (2 mM), penicillin (100 units/mL), sodium pyruvate (1 mM), streptomycin (100 μg/mL) and NS21 (Chen et al., 2008). Two times a week, fresh medium was added and GCM was harvested after 2 weeks. GCM was spun down (5 min at 3000 *g*) to remove cellular debris. Two thirds of the RGC medium were replaced by GCM. To induce accumulation of unesterified cholesterol, RGCs were treated with 3-β-[2-(diethylamine)ethoxy]androst-5-en-17-one (U18666A; Interchim) after two days in culture at a concentration of 0.5 μg/mL for 48 h. The drug induces cholesterol accumulation in cells (Karten et al., 2002; Liscum and Faust, 1989) by blocking NPC1 activity (Lu et al., 2015). Cultures were treated for 24 h with indicated concentrations of CD [MW ~1400; 50 μM ~ 70 μg/mL ~ 0.007% (*w/v*)] and with CDAuNPs.

2.3. Intravitreal injections

CD (100 mM; Sigma H5784) or CDAuNPs (~100 mM CD) and vehicle (PBS) were administered by intravitreal injections in 4-weeks-old animals. To this end, mice were anesthetized by isoflurane inhalation (3% for 15 min) and injected using glass micropipettes and a micro-injector (Picospritzer III, Parker Hannifin, Pine Brooks, NJ, USA) in the right and left eye with drug and vehicle, respectively (volume 1 μL). One hour after injection, eyes were treated with gel to lubricate and rehydrate the cornea (Ocry-gel, TVM Lab) and mice were returned to their cage. For technical reasons, multiple intravitreal injections were not possible and observations were limited to a time period of 48 h, before molecules are completely eliminated from the retina (Del Amo et al., 2017; Schmitt et al., 2019; Varadi et al., 2019). At indicated time points after injections, animals were deeply anethetized by intraperitoneal injections of 100 mg/kg ketamine and 20 mg/kg xylazine prior to dissection of eyeballs or retinae and euthanized by decapitation immediately after.

2.4. Histochemical and immunohistochemical staining

Eyeballs were rapidly removed from mice and immersion fixed using paraformaldehyde (45 min in PBS for 30 min) after an incision along the ora serata to remove the cornea. For whole-mount staining, retinae were dissected and processed in 96-well plates. For staining of retinal sections, eyeballs were embedded in agarose (5% in PBS), and cut at 50 μm thickness on a vibratome (Leica, VT1000S). For immunohistochemical staining, retinal tissue was blocked using bovine serum albumin (BSA, 2%) and goat serum (5% in PBS) and permeabilized (0.1% Triton X-100 with 0.1% BSA in PBS) for 45 min and incubated overnight at 4 °C with primary antibodies (diluted in 1% BSA, 1% goat serum in PBS). Sections were washed and incubated for 2 h at RT with secondary Alexa-labelled antibodies (1:500 in PBS). The following antibodies were used for immunohistochemical staining: anti-Tuj1 (1:1000; Covance; MMS-435P-250), anti-IBA1 (1:500; Wako; 019–19,741), anti-GFAP (1:200; Sigma; G3893), anti-CD68 (1:100; Biorad; MCA1957), anti-MPO (1:500; Dako; A0398). For nuclear staining, retinal sections were incubated for 10 min with Sytox Green (0.25 μM; Invitrogen). Fluorescence images of retinal sections or whole-mounts were acquired on a confocal microscope (Leica SP5 II, Leica Microsystems) or an inverted microscope (Zeiss Observer 7) equipped with objectives (40× water, N.A. 1.2; 63× oil, N.A. 1.4), a module for optical sectioning by structured illumination (Zeiss ApoTome.2) and a digital camera (Hamamatsu ORCA-Flash 4.0). The size and density of glial cells were analysed semi-automatically using ImageJ and the Map_BoneMicrostructure plugin (National Institutes of Health, Bethesda, MD).

2.5. Detection and quantification of cholesterol accumulation by filipin staining

To visualize unesterified cholesterol in cultured RGCs, cells were fixed by paraformaldehyde (4% in PBS for 15 min at RT) and stained with filipin (50 μg/mL in PBS for 2 h at RT; from 250-fold ethanolic stock solution; F9765, Sigma). Fluorescence images of cultured cells were acquired using an inverted microscope (Axiovert 135TV; Zeiss) equipped with a metal halide lamp (10%; Lumen 200; Prior Scientific), an appropriate excitation/emission filter (XF02–2; Omega Optical Inc.), a 40× objective (oil, N.A. 1.3; Zeiss) and an air-cooled monochrome charge-coupled device camera (Sensicam, PCO Computer Optics) controlled by custom-written Labview routines (National Instruments). For histochemical detection of unesterified cholesterol, fixed retinal vibratome sections were incubated for 1 h with filipin (10 μg/ml in PBS) and digital images were aquired using an inverted microscope (Zeiss Observer 7; 40× water objective; ApoTome.2; Hamamatsu ORCA-Flash 4.0). To estimate the level of cholesterol accumulation, the density of filipin-positive puncta in images was determined semi-automatically by a custom-written Labview routine (Demais et al., 2016). Briefly, regions of interest covering neuronal somata (*in vitro* or in retinal layers) and retinal tissue in plexiform layers were outlined manually by circles and rectangles, respectively in micrographs. To detect fluorescent puncta, regions of interest were processed by a Mexian hat filter to enhance puncta-like features, segmented using a median intensity-derived threshold and subjected to particle detection with a minimum size of 3 pixels. The density of filipin-positive puncta per regions of interest was calculated as number of particles per area normalized to 10,000 square pixels.

2.6. TEM

For ultrastructural analyses, retinae were fixed with glutaraldehyde (2.5% in 0.1 M cacodylate buffer at pH 7.4 for 2 h at RT; Electron Microscopy Services-EMS) and rinsed with cacodylate buffer. Cholesterol was stained by filipin (50 μg/ml for 30 min, from a 100-fold dimethylformamide stock solution). Retinal sections were postfixed for 1 h with osmium tetroxide [OsO_4; 2%(*w/v*)] in 100 mM imidazole buffer to enhance lipid preservation before dehydration, embedding, and

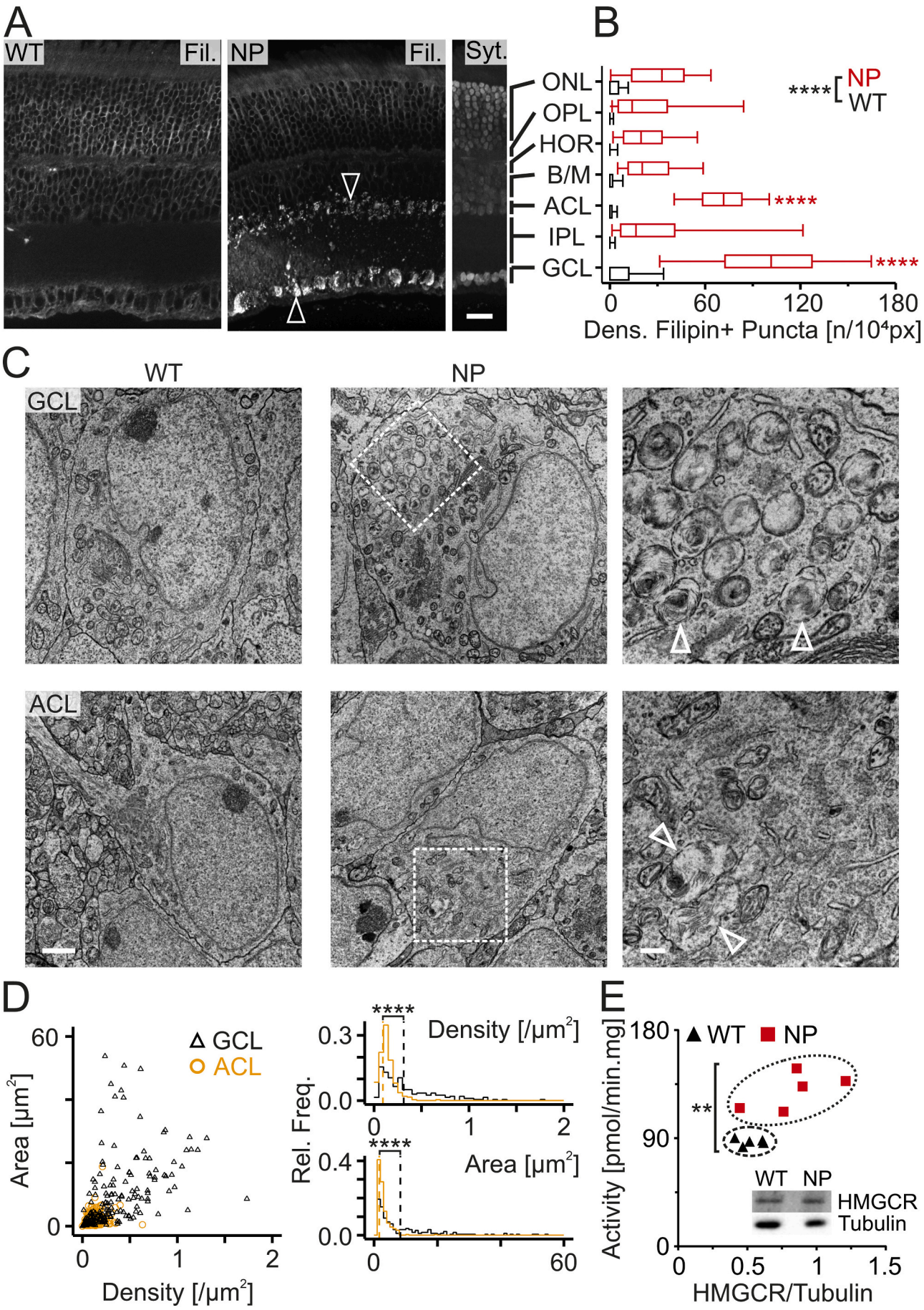

(caption on next page)

Fig. 1. Pathologic accumulation of cholesterol in retinae of NPC1-deficient mice.
A, Fluorescence micrographs of retinal sections from 4-weeks-old wild-type (WT) and NPC1-deficient (NP) mice subjected to staining with filipin (Fil., left and middle micrograph) and Sytox green to label nuclei (Syt., right micrograph). ONL, outer nuclear layer; OPL, outer plexiform layer; HOR, horizontal cells; B/M, bipolar cells and Müller cells; ACL, amacrine cell layer; IPL, inner plexiform layer; GCL, ganglion cell layer. Arrowheads indicate cells in the GCL and ACL with strong accumulation of unesterified cholesterol (bright filipin signal). Scale bar: 50 μm. B, Boxplots showing densities of filipin-positive puncta in indicated retinal layers of WT and NP mutant mice. In all layers, densities in NP mice were significantly higher compared to those in WT mice (black asterisk). In NP mice, densities in the GCL and ACL were significantly higher than those in all other layers [red asterisks; two-way ANOVA followed by Tukey's post-hoc test; $F(6, 2103) = 116.7$; 37–620 regions of interest from 4 WT or NP mice]. C, Transmission electron micrographs showing representative neuronal somata in the GCL and ACL from WT and NP mice. Note the presence of lamellar inclusions (indicated by arrowheads) in NPC1-deficient neurons. Scale bars: 2 μm (left, middle), 500 nm (right). D, Scatterplots (left) and relative frequency histograms (right) of the density and the area of inclusions present in neuronal somata of the GCL (black, NP: 5 animals/200 cells) and of the ACL (orange, NP: 5/248) from NPC1-deficient retinae. Dashed vertical lines indicate mean values. Asterisks indicate statistically significant differences between the two layers (Wilcoxon rank-sum test; density: $W = 37{,}231$; area: $W = 37{,}058$; non-normally distributed values indicated by Shapiro-Wilk normality test; density: $W = 0.83$; area: $W = 0.85$; $p < 0.0001$). E, Scatterplots of enzyme activity and normalized protein levels of 3-hydroxy-3-methylglutaryl-Coenzyme A reductase (HMGCR) in retinae from WT and NP mice indicating an increase of cholesterol synthesis due to NPC1-deficiency. Insert, representative immunoblot showing levels of HMGCR and of tubulin used as loading control. Asterisk indicates statistically significant increase in enzyme activity due to NPC1 deficiency [independent samples *t*-test: $t(4) = -6.1$; $n = 5$ mice; unequal variance; F test: $F(4) = 0.033$; $p < 0.01$].(For interpretation of the references to color in this figure legend, the reader is referred to the web version of this article.)

ultramicrotomy. To detect CDAuNPs, retinal sections were fixed with glutaraldehyde (2.5% in PBS at pH 7.4 for 1 h at RT; Electron Microscopy Services-EMS), rinsed with PBS and then with double-distilled water. Gold particles were silver enhanced using the R-Gent SE-EM kit (Aurion). Sections were postfixed in OsO_4 (0.5% in aqua bidestillata for 15 min), dehydrated in graded ethanol series and embedded in Embed 812 (EMS). Ultrathin sections were cut with an ultramicrotome (Leica), stained with uranyl acetate [1% (w/v) in 50% ethanol], and examined with a Hitachi H7500 transmission electron microscope equipped with a digital camera (Advanced Microscopy Techniques/Hamamatsu). Quantitative measurements were obtained manually from electron micrographs.

2.7. 3-hydroxy-3-methylglutaryl-Coenzyme A reductase (HMGCR) activity assay

The assay was performed by the radioisotopic method based on the production of [^{14}C]MVA from 3-[^{14}C]-HMG-CoA (specific activity 57.0 mCi/mmol., Amersham-Pharmacia, Little Chalfont, UK) as described (Segatto et al., 2014). Briefly, retinae were homogenized (1:5 w/v) in PBS containing (in mM) 100 sucrose, 50 KCl, 40 KH_2PO_4, 30 EDTA, pH 7.4 and incubated in the presence of co-factors (20 mM glucose-6-phosphate, 20 mM NADP sodium salt, 1 unit of glucose-6-phosphate dehydrogenase and 5 mM dithiothreitol). The assay was started by the addition of 3-[^{14}C]-HMG-CoA (0.088 μCi/11.7 nmol). The newly synthesized [^{14}C]-MVA was purified by ion exchange chromatography (AG1-X8 resin; BioRad Laboratories) and its radioactivity was measured by a liquid scintillation counter (Perkin Elmer 2100TR). An internal standard (3-[^{3}H]-MVA, specific activity 24.0 Ci/mmol., Amersham-Pharmacia) was added to calculate recovery. HMGCR activity was expressed as pmol/min/mg protein.

2.8. Tissue lysate preparation and immunoblotting

Total lysate of retinae was obtained by tissue homogenization in 1:5 w/v homogenization buffer (in mM 10 Tris-HCl, 1 $CaCl_2$, 150 NaCl, 1 PMSF, pH 7.5). The samples were sonicated (VCX 130 PB, Sonics) on ice for 30 s, and centrifuged for 7 min at 13,000 rpm at 4 °C to yield total lysate, which was boiled for 5 min before SDS-PAGE and subsequent immunoblotting. Proteins were separated by SDS–PAGE and blotted to nitrocellulose membranes (Trans-blot Turbo, BioRad). Immunoblots were incubated with anti-HMGCR primary antibody (Upstate; 1:500) overnight, followed by secondary peroxidase-conjugated antibodies produced in rabbit (1:10,000; Biorad). Immunoreactivity was detected by enhanced chemiluminescence (GE Healthcare). As loading control, the immunoblots were reacted with an antibody against tubulin (1:10,000; Sigma Aldrich). Band intensities were quantified using ImageJ (National Institutes of Health, Bethesda, MD).

2.9. Data analysis

Data analysis, visualization and statistical tests were accomplished with the open source software R (R Core Team, 2021) and selected packages (ggplot2: Wickham, 2016; ggbeeswarm: Clarke and Scott-Sherrill-Mix, 2017). Statistical tests were performed as indicated. Parametric tests were used except for measures, where the non-normal value distribution could be established. Where possible, drug effects were examined based on data from ipsi-/drug- and contra-lateral/vehicle-injected eyes using within-subject (repeated measures) tests. Asterisks indicate statistically significant differences based on *p* values (*, $p < 0.05$; **, $p < 0.01$; ***, $p < 0.001$; ****, $p < 0.0001$).

3. Results

We studied the immediate effects of CD on retinal neurons *in vivo* using intravitreal drug injections in NP and WT mice at 4 weeks of age before the onset of neurologic symptoms.

3.1. Pathologic cholesterol accumulation in retinae of NPC1-deficient mice

First, we examined the distribution of unesterified cholesterol in retinae of 4-weeks-old mice. Previous studies noted lipid accumulation in retinae of NP mice at 2 months of age (Claudepierre et al., 2010; Palladino et al., 2015; Yan et al., 2014a), but the situation in younger animals remained unknown. Histochemical staining of retinal sections revealed the presence of filipin-positive puncta in all layers of 4-weeks-old NP mice, and their absence from retinae of wild-type (WT) littermates. The highest densities were found in the ganglion cell and amacrine cell layer (Fig. 1A, B). Inspection of retinal sections by TEM revealed the presence of lamellar inclusions in retinal neurons from NP mice and their absence from retinae of WT littermates (Fig. 1C) as shown

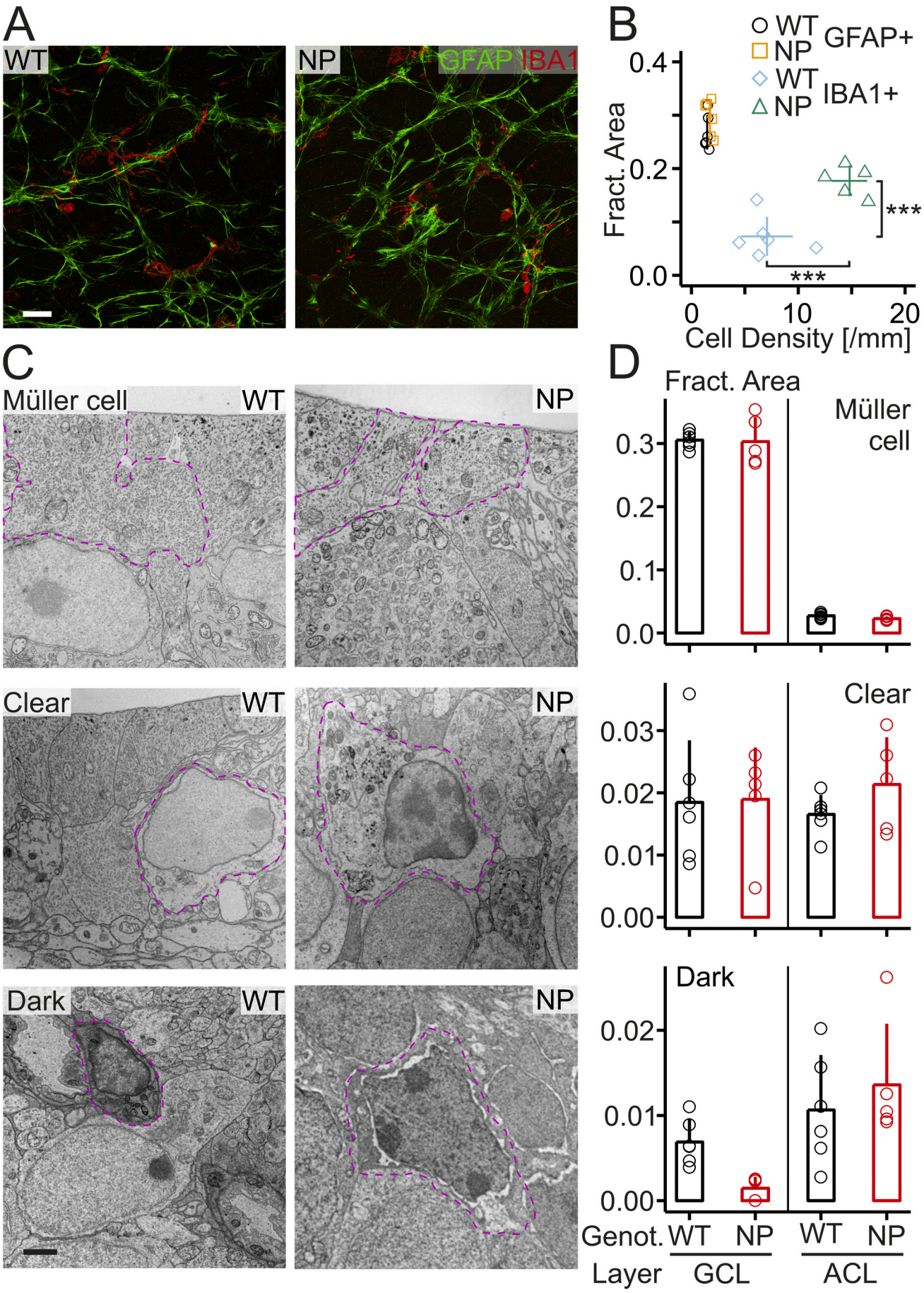

(caption on next page)

Fig. 2. Glial reaction to NPC1 deficiency in retinae of 4-weeks-old mice.
A, False-color fluorescence micrographs showing the distribution of the glial cell markers GFAP (astroglia type) and IBA1 (microglia type) in retinal whole-mounts from wild-type (WT) and NPC1-deficient (NP) mice. Scale bar: 25 μm. B, Scatterplots of the mean fractional area and of the mean density of glial cells positive for the indicated markers in individual mice with the indicated genotype. Asterisks indicate statistically significant changes in IBA1-positive cells due to NPC1 deficiency [independent samples t-test, equal variance; density: $t(9) = -6.1$; fractional area: $t(9) = -5.1$; WT: $n = 6$; NP: $= 5$]. C, Electron micrographs with magenta lines indicating selected Müller cell endfeet and glial cells with clear (astroglia-type) and dark (microglia type) cytoplasm in retinae of WT and NP mice. Scale bar: 2 μm. D, Mean fraction of cytoplasmic area (excluding nuclei) occupied by indicated glial cells in the ganglion cell layer (GCL) and amacrine cell layer (ACL) from WT and NP animals. Columns and whiskers indicate mean and standard deviation, respectively. No statistically significant differences between NP and WT mice were detected in the fractional areas of the different types of glial cells in the GCL or ACL [$p > 0.05$; two-way ANOVA; clear: $F(1,18)$ 0.4; dark: $F(1, 18) = 3.8$; Müller: $F(1, 18) = 0.01$; WT: $n = 6$; NP: $n = 5$].

previously in older animals (Claudepierre et al., 2010; Yan et al., 2014a). Notably, we observed layer-specific differences: Neurons in the GCL had more and larger inclusions than those in the amacrine cell layer (ACL; Fig. 1D). In line with neuron-specific transcriptional changes due to NPC1 deficiency (Demais et al., 2016), the disturbed cholesterol flow within retinal cells induced an upregulation of cholesterol synthesis as indicated by enhanced activity and protein level of the rate-limiting enzyme, HMGCR (Fig. 1E). Together, these results revealed layer-specific accumulation of cholesterol in retinal neurons of presymptomatic mice and thus validated their use to explore the effects of CD on retinal neurons.

3.2. Reaction of retinal glia to NPC1-deficiency

We asked how retinal glial cells react to the absence of NPC1 in 4-weeks-old mice. Immunohistochemical staining of retinal whole-mounts revealed increased densities and areas of IBA1-positive microglial cells in retinae of NP mice compared to those from WT littermates. However, no changes were observed for GFAP-positive cells at this age (Fig. 2A, B). These findings are in line with observations that microglial activation precedes the reaction of GFAP-positive cells in brains of *Npc1* mutant mice (Baudry et al., 2003; German et al., 2002; Maulik et al., 2012; Park et al., 2019). Next, we examined the ultrastructural changes in glial cells of the GCL and ACL, where neurons showed strong cholesterol accumulation. The fractional area covered by Müller cells and glial cells with clear (Fig. 2C) and dark cytoplasm (Fig. 2D) was not significantly affected by NPC1 deficiency in 4-weeks-old animals. Based on established ultrastructural criteria (Bisht et al., 2016; Kavetsky et al., 2019; Peters et al., 1991; Ramírez et al., 1996) cells with clear and dark cytoplasm correspond to astrocytes and microglial cells, respectively. Lamellar inclusions were absent from retinal Müller cells in NP mice (total of 2410 μm^2 and 1486 μm^2 for $n = 6$ WT and $n = 6$ NP mice) in line with a previous study (Palmer et al., 1985). They were also not detectable in glial cells with clear and dark cytoplasm, which covered relatively small areas of the GCL and ACL regardless of the genotype. Together, these results revealed minor changes in retinal glial cells of NPC1-deficient presymptomatic mice.

3.3. Reduction of cholesterol accumulation in retinal neurons following direct delivery of CD

Next, we used intravitreal injections to study how CD impacts cholesterol accumulation in retinal neurons most affected by NPC1 deficiency *in vivo*. As control, contralateral eyes were injected with vehicle (PBS). Filipin staining of retinal sections showed that within 24 and 48 h a single injection of CD reduced the extent of cholesterol accumulation in neurons of the ACL and GCL from mutant mice compared to vehicle (Fig. 3A, B). Inspection of NPC1-deficient neurons by TEM revealed that CD reduced the density of inclusions filled with lamellae, named full inclusions, and induced the presence of inclusions bearing few lamellae, named half-full inclusions, or lacking them altogether, named empty inclusions (Fig. 3C). The quantitative analysis indicated layer-specific neuronal reactions to CD: in the GCL, the area covered by full inclusions decreased and half-full and empty counterparts appeared and covered similar fractional areas. In the ACL, full inclusions largely dissappeared and half-full inclusions predominated with little contribution from empty inclusions (Fig. 3D). The appearance of inclusions with few or no lamellae was in line with our findings *in vitro* that CD induces a partial redistribution of cholesterol within neurons (Demais et al., 2016). In addition to inclusions with distinct lamellar content, we also observed inclusions that were seemingly located in between two neurons and that were not enveloped by the plasma membrane of either cell (Fig. 3E). This observation supported our hypothesis that CD induces the release of inclusions to the extracellular space (Demais et al., 2016).

3.4. Tracking CD with gold nanoparticles

We hypothesized that CD removes cholesterol from inclusions thus permitting its partial incorporation into the cellular pool. Such action would require that CD reaches the interior of lamellar inclusions. To locate CD in subcellular compartments, we coupled CD to 2.5 nm gold nanoparticles. These particles can be visualized by TEM, and they have been used extensively in eye research (Masse et al., 2019). Analyses of CDAuNPs by high resolution TEM combined with energy-dispersive X-ray spectroscopy revealed the presence of monodispersed particles with a narrow size distribution (radius 2.6 ± 0.7 nm; $n = 1000$; Fig. 4A) and confirmed the presence of carbon and gold (Fig. 4B). To ensure that CD coupled to AU particles retains the ability to reduce cholesterol accumulation due to NPC1 dysfunction we first performed experiments using serum-free primary cultures of purified RGCs. These *in vitro* tests confirmed that CDAuNPs reversed the U18666A-induced accumulation of cholesterol in neurons as efficiently as CD (Fig. 4C). We next injected CDAuNPs intravitreally in NP mice and traced their fate by TEM. CDAuNPs were present in lamellar inclusions of cells in the GCL already starting from 2 h after injection suggesting their *in vivo* uptake *via* the endosomal-lysosomal system (Fig. 4D). We also found particles in the cytoplasm of Müller cells and in blood vessels at 24 h after injection in NP mice (Fig. 4E).

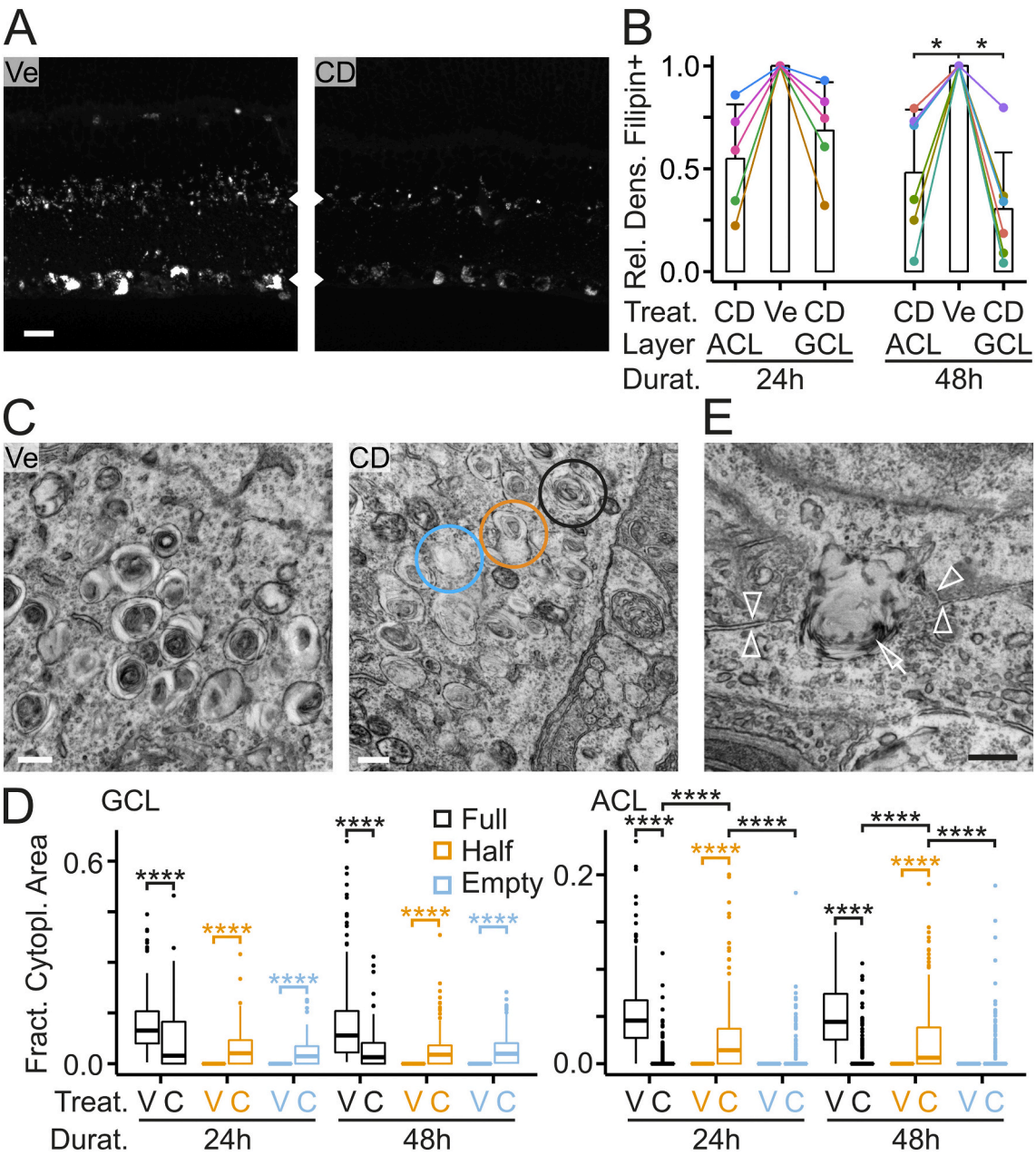

Fig. 3. CD-induced reduction of cholesterol accumulation in NPC1-deficient retinal neurons *in vivo*.
A, Fluorescence micrographs of filipin-stained retinae from NPC1-deficient (NP) mice 24 h after intravitreal injections of PBS (vehicle, Ve) or 2-hydroxypropyl-beta-cyclodextrin (CD). Arrowheads indicate the amacrine cell layer (ACL, top) and the ganglion cell layer (GCL, bottom). Scale bar: 25 μm. B, Effect of CD on the density of filipin-positive puncta in neuronal somata of the indicated layers from individual NP mice normalized to vehicle-treated contralateral eyes. Values were measured at indicated time periods after injections. Bars and whiskers indicate the mean and standard deviation, respectively. Circles represent values from indicated layers of individual mice connected by lines. Asterisks indicate statistically significant changes (Wilcoxon signed rank test; 48 h: V = 21 for GCL and ACL). C, Representative electron micrographs of lamellar inclusions observed in neurons of the GCL of NP mice at 24 h after intravitreal injection of vehicle and CD. CD treatment induced the occurrence of inclusions without lamellae (empty, sky blue) and with lamellae filling approximately half of their interior (half, orange) in NP mice. Inclusions with lamellae filling the entire interior are also indicated (full, black). Scale bar: 500 nm. D, Boxplots showing the fractional cytoplasmic area occupied by the different types of inclusions in neuronal somata of the GCL [left, 24 h Vehicle $n = 4$ animals/192 cells; CD: 4/124; 48 h: V: 6/261; C: 5/171] and of the ACL (right, 24 h: V: 4/311; C: 4/206; 48 h: V: 6/327; C: 5/284). CD-induced changes in the fractional cytoplasmic area covered by different types of inclusions were statistically significant compared to vehicle-treated eyes. In the GCL of CD-treated animals, the three types of inclusions covered similar areas, whereas in the ACL, half full inclusions predominated covering significantly larger areas than full and empty inclusions [three-way ANOVA followed by Tukey's post-hoc test; GCL: $F(2,2232) = 5.4$; ACL: $F(2, 3368) = 2.4$]. E, Electron micrograph showing a lamellar inclusion (arrow) that is located at the border between two neurons in the GCL, but not enveloped by the plasma membrane of either cell (arrowheads). The observation suggests the CD-induced release of the inclusion from neurons. The image was obtained from the retina of a NP mouse 24 h after intravitreal injection of CD. Scale bar: 500 nm.(For interpretation of the references to color in this figure legend, the reader is referred to the web version of this article.)

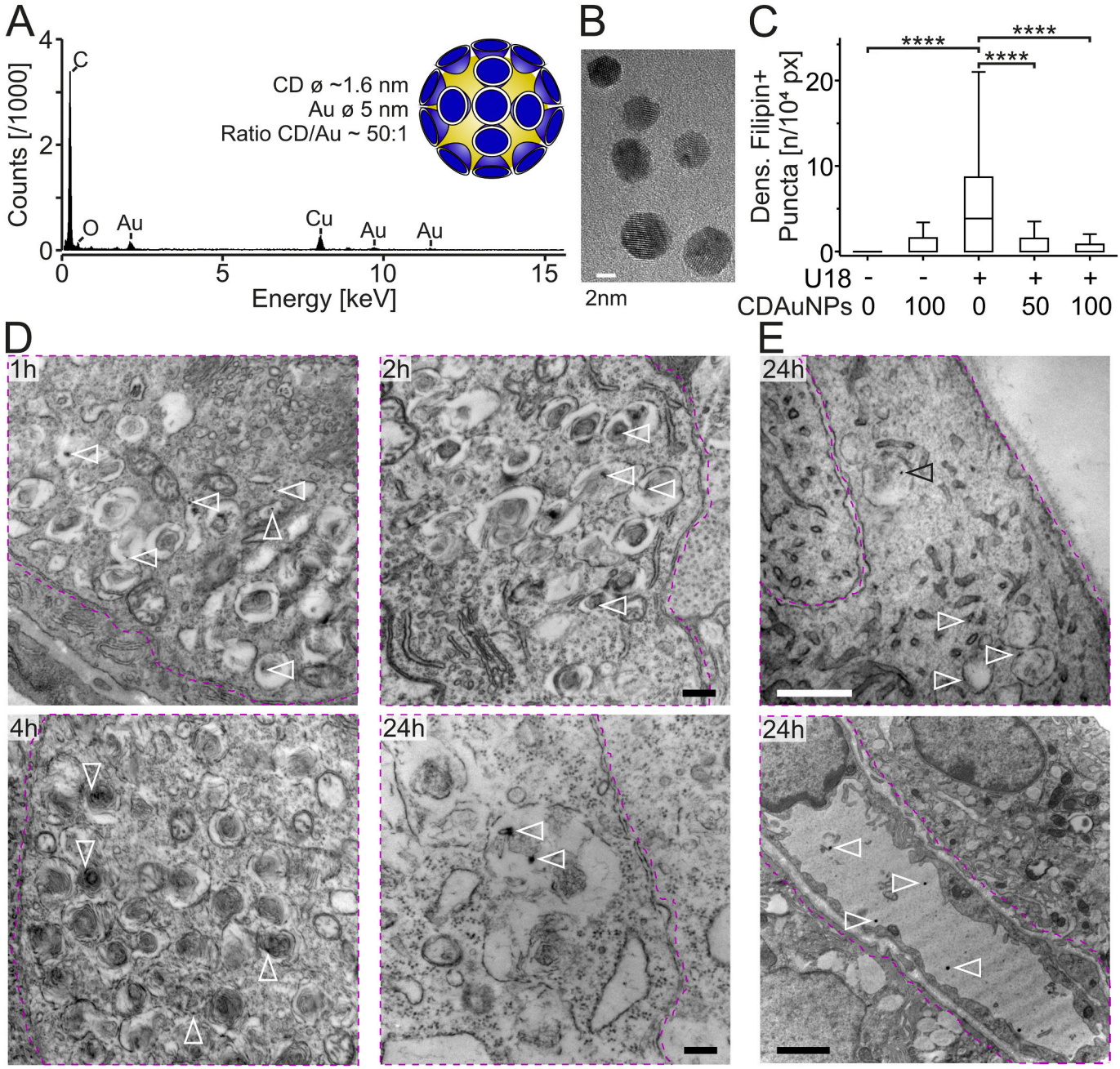

Fig. 4. Tracking the subcellular localization of CD with gold. (For interpretation of the references to color in this figure legend, the reader is referred to the web version of this article.)

A, Elementary composition of 2-hydroxypropyl-beta-cyclodextrin gold nanoparticles (CDAuNPs) as shown by energy-dispersive X-ray spectroscopy. Detected chemical elements include carbon (C), oxygen (O), gold (Au) and copper (Cu). The Cu peak is due to copper grids used for TEM inspection. Inset, schematic view of CDAuNPs (approximately to scale). B, Electron micrograph of CDAuNPs. C, Bloxplots showing the density of filipin-positive puncta in somata of highly purified retinal ganglion cells (RGCs) cultured under indicated conditions with and without induction of cholesterol accumulation by U18666A (U18; 0.5 μg/mL for 48 h). Concentrations of CDAuNPs are indicated in μM (-U18/CDAuNPs 0: $n = 191$ cells; -U18/CDAuNPs 100: 129; +U18/CDAuNPs 0: 215; +U18/CDAuNPs 50: 194; +U18/CDAuNPs 100: 178). The U18-induced increase in the density of filipin-positive puncta was reverted by CD and CDAuNPs [two-way ANOVA followed by Tukey's post-hoc test; $F(1, 902) = 101.0$]. D and E, Electron micrographs of retinae from NP mice showing – outlined in magenta – the cytoplasm of neurons in the ganglion cell layer (GCL, D), the cytoplasm of Müller cell end feet apposed to the vitreous (E, top) and a blood vessel (E, bottom) at indicated times following intravitreal injection of CDAuNPs. Arrowheads indicate the presence of CDAuNPs in lamellar inclusions of neurons (D), the cytoplasm and vesicular structures of Müller cell endfeet (E, top) and the lumen of a blood vessel (E, bottom). Scale bars: 500 nm (D; E, top), 2 μm (E, bottom).

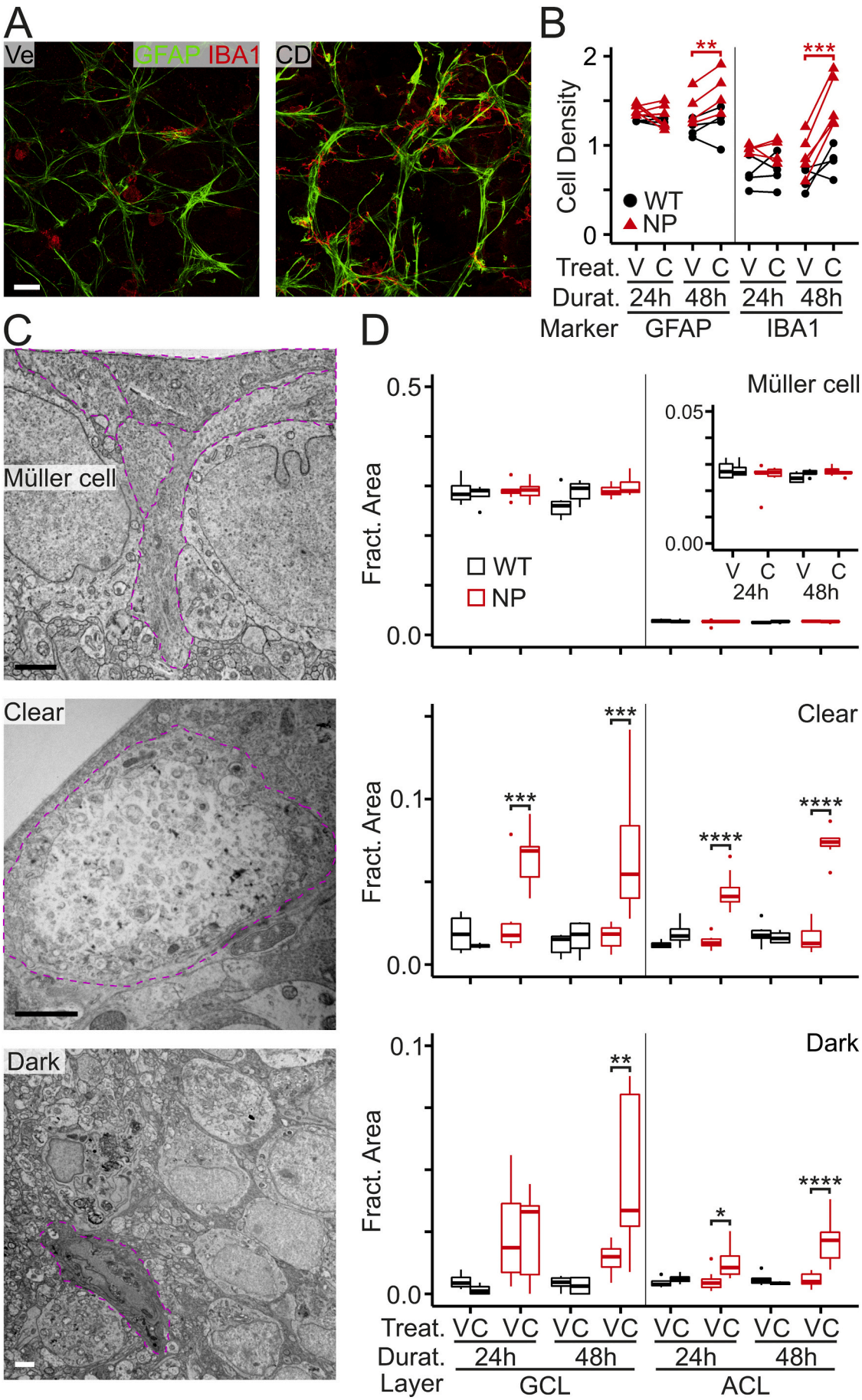

(caption on next page)

Fig. 5. Reaction of retinal glial cells to intravitreal injections of CD.
A, False-color fluorescence micrographs of retinal whole-mounts from NPC1-deficient (NP) mice 48 h after intravitreal injection of PBS (vehicle, Ve) or 2-hydroxypropyl-beta-cyclodextrin (CD) and immunohistochemical staining for GFAP- (green; astroglia type) and IBA1- (red) positive cells (microglia type). Scale bar: 25 μm. B, Density of GFAP- and IBA1-positive cells in retinal whole-mounts of wild-type (WT) and NP mice at indicated times after intravitreal injection of vehicle (V) and CD (C) in the left and right eye, respectively. CD induced statistically significant changes after 48 h in NP mice, but not in WT littermates [repeated measures two-way ANOVA; GFAP: $F(1,13) = 6.6$; IBA1: $F(1,11) = 15.6$; followed by paired *t*-test; GFAP: $t(3) = -6.6$; IBA1: $t(4) = -10.3$]. C, Representative electron micrographs of Müller cell endfeet and glial cells with clear and dark cytoplasm (outlined by magenta lines) in retinae of NP mice after intravitreal injection of CD. Scale bar: 2 μm. D, Boxplots showing area covered by indicated glial cells as fraction of total area analysed in the retinal ganglion cell layer (GCL) and amacrine cell layer (ACL) per mouse with indicated genotypes at indicated times after intravitreal injections of vehicle (V) or CD (C; 24 h WT Vehicle/CD: $n = 4/4$ animals, NP V/C: 10/9; 48 h WT V/C: 6/6, NP V/C: 8/7). Inset, fractional area of Müller cells in ACL at modified scale. CD induced statistically significant changes in clear and dark glial cells from NP mice [three-way ANOVA followed by Tukey's post-hoc test; Müller, GCL: $F(1, 46) = 1.4$; ACL: $F(1, 46) = 1.4$; clear, GCL: $F(1, 46) = 0.01$; ACL: $F(1, 46) = 17.2$; dark, GCL: $F(1, 46) = 2.9$; ACL: $F(1, 46) = 3.4$].(For interpretation of the references to color in this figure legend, the reader is referred to the web version of this article.)

3.5. Reaction of retinal glia to intravitreal administration of CD

Next, we studied how glial cells react to intravitreal injections of CD in WT and NP mice. Immunohistochemical staining of retinal whole-mounts revealed an increased density of GFAP- and IBA1-positive cells 48 h after injection of CD, but not of vehicle. Notably, these changes were only observed in NP, but not in WT animals (Fig. 5A, B). Inspection of retinae by TEM showed layer- and cell type-specific responses of glial elements to CD injections in NP mice. CD strongly increased the fractional area covered by glial cells with clear cytoplasm in the GCL and ACL of NP mice at 24 and 48 h after injections (Fig. 5C, D). Glial cells with dark cytoplasm reacted similarly, but the expansion was more marked at 48 h after the injection (Fig. 5C, D). Notably, Müller cells from NP mice did not show noticable changes in fractional area in response to injections (Fig. 5C, D). Moreover, no changes in area covered by glial elements were observed in WT mice or after vehicle injections.

3.6. CD-induced presence of lamellar inclusions in glial cells in vivo

Our previous work *in vitro* (Demais et al., 2016) together with our ultrastructural observations in retinae of CD-injected mice (Fig. 3E) suggested that CD enables neurons to release lamellar inclusions into the extracellular space. If this was the case, what would be their fate? The lamellar inclusions released from neurons may have been taken up by glial cells. Histochemical and immunohistochemical staining of unesterified cholesterin and glial cells, respectively revealed increased colocalization of filipin-stained cholesterol in GFAP- and IBA1-positive cells in retinae from NP-deficient mice following intravitreal injections of CD compared to vehicle (Fig. 6A). TEM revealed that CD strongly increased the size of phagosome-like structures in both clear and dark glial cells in the GCL and ACL of NP animals and that these phagosomes contained exclusively lamellar inclusions (Fig. 6B, C). These changes were not induced by vehicle, and they were absent from WT animals (Fig. 6C). Together, our results indicated that CD induces an uptake of lamellar inclusions by glial cells leading to a strong expansion of the area covered by glial elements.

3.7. CD-induced presence of neutrophil granulocytes in retinae of NPC1-deficient mice

Observation of retinal sections from CD-injected NP mice by TEM revealed the presence of cells with characteristic features of neutrophil granulocytes. These include a diameter of 12–15 μm, polymorph nuclei rich in heterochromatin and granule-rich cytoplasm (Duvvuri et al., 2020; Yipp et al., 2012) (Fig. 7A). To follow up on this, we performed immunohistochemical stainings of retinae with MPO, a marker of neutrophil granulocytes, and CD68 to discern microglial cells (Fig. 7B). These experiments showed that CD enhanced the density of MPO-positive and CD68-negative cells in NP mice, whereas this change occurred more rarely in vehicle-injected animals or in WT mice (Fig. 7C). Neutrophil granulocytes seemed predominantly located in the nerve fiber layer and GCL. Quantitative ultrastructural analysis confirmed the their appearance and their layer-specific localization upon CD injection (Fig. 7D). These findings suggested that CD induces the entry of neutrophil granulocytes into retinae of NP mice.

4. Discussion

Using the mouse retina as experimental model and intravitreal injections as mode of drug administration we provide new insight how CD reverts cholesterol accumulation in NPC1-deficient neurons *in vivo*. Our results indicate that CD is rapidly taken up by neurons and enters lamellar inclusions. This was shown by new CDAuNPs enabling ultrastructural detection of CD. The conjugates are likely to behave similarly to CD. Previous reports showed cellular uptake of cyclodextrins coupled to dextran (Rosenbaum et al., 2010), a bodipy fluophore (Dai et al., 2017), fluorescein (Plazzo et al., 2012) and fluorescent nanoparticles (Donida et al., 2020) *in vitro*. Our control experiments confirmed similar efficacy of CDAuNPs and CD in reducing the cholesterol accumulation in NPC1-deficient neurons. CD reduced the density of lamellae inside inclusions suggesting that the compound enables a partial exit of cholesterol and possibly other lipids from these structures independently from NPC1 (Abi-Mosleh et al., 2009). This may involve alternative shuttle mechanisms (Heybrock et al., 2019). Our observation that CD acts inside cells is supported by findings *in vitro* that the molecule reduces cholesterol accumulation with cell-specific delays (Dai et al., 2017; Meske et al., 2014) and that endocytotic uptake is required for its action (Rosenbaum et al., 2010; Vance and Karten, 2014). The continued presence of lamellae inside inclusions may be caused by *de novo* formation or by lipids that are not affected by CD. The layer-specific differences in the size and density of lamellar inclusions and in the reaction to CD treatment suggest neuron-specific modes or rates of lipid accumulation and of their CD-mediated clearance.

Previous *in vitro* studies on NPC1-deficient cell lines showed that cyclodextrin induces the secretion of cholesterol ((Argüello et al., 2021) Chen et al., 2010; Feltes et al., 2020; Vacca et al., 2019) probably by distinct mechanisms depending on the different cell lines and experimental conditions used. This included transfer to serum-resident

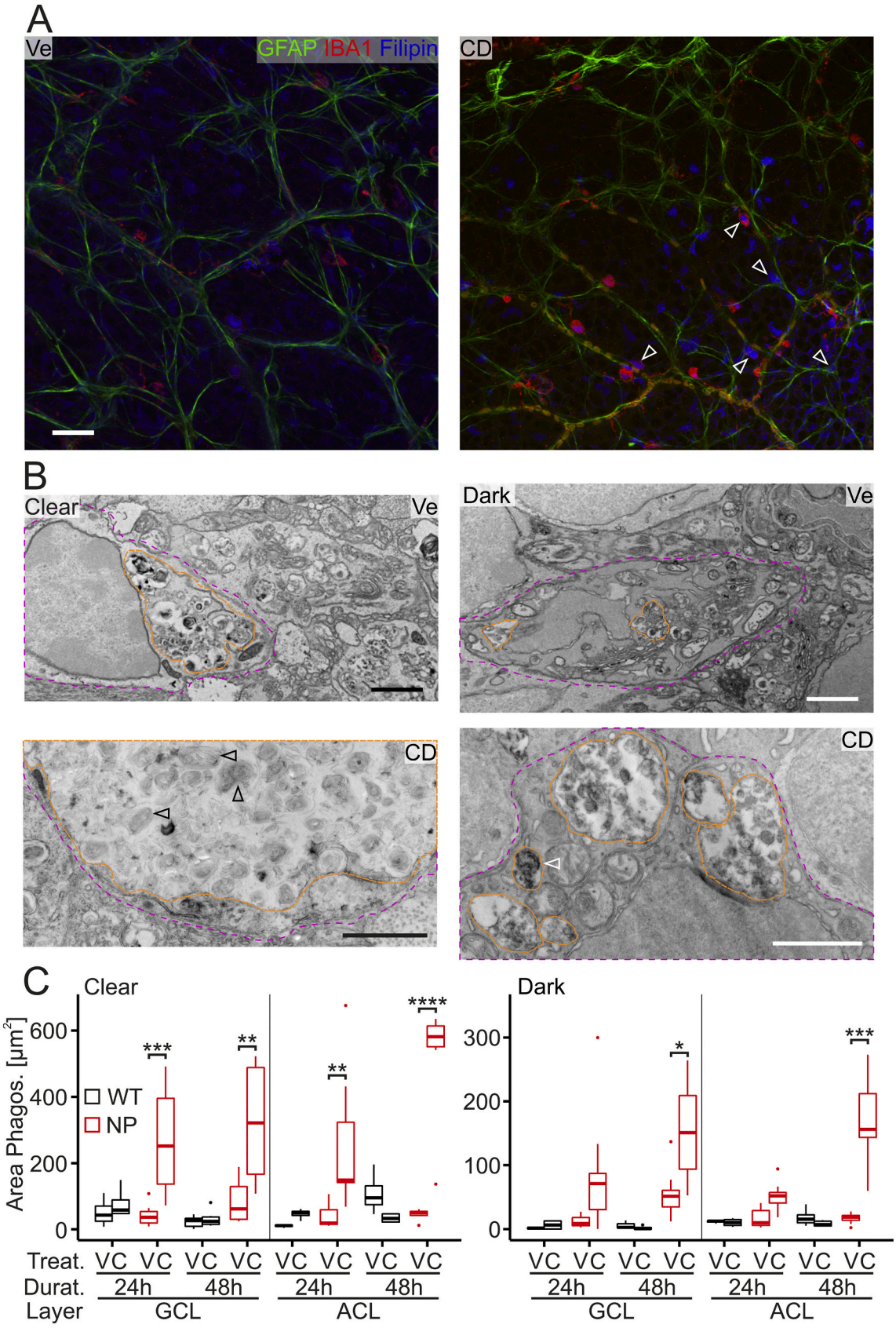

(caption on next page)

Fig. 6. CD-induced uptake of lamellar inclusions by glial cells *in vivo*.
A, Representative false-color fluorescence micrographs showing increased presence of filipin-stained unesterified cholesterol (blue) in somata of GFAP- (green) and IBA1-positive (red) cells (arrowheads) in retinal whole-mounts from NPC1-deficient (NP) mice at 24 h after intravitreal injections of 2-hydroxypropyl-beta-cyclodextrin (CD). Less filipin staining was observed in retinal glial cells from vehicle- (Ve-) injected contralateral eyes. Scale bar: 25 μm. B, Representative electron micrographs of phagosome-like structures (orange outlines) in clear (left; magenta outline; astroglia-like) and dark (right; magenta outline; microglia-like) glial cells in retinae from NP mice at 48 h after intravitreal injection of vehicle (Ve, top) and CD (bottom). Note that following CD injections, phagosomes were strongly enlarged and contained almost exclusively lamellar inclusions indicated by arrowheads. Scale: 500 nm. C, Boxplots showing the area covered by phagosomes in clear (left) and dark (right) glial cells in the retinal ganglion cell layer (GCL) and amacrine cell layer (ACL) from wild-type (WT) and NP animals at indicated times after intravitreal injections of vehicle (V) or CD (C) in the left and right eye, respectively (24 h WT Vehicle/CD: $n = 4/4$ animals, NP V/C: 10/9; 48 h WT V/C: 6/6, NP V/C: 8/7). CD induced a time and layer-specific enlargement of glial phagosomes in NP mice [three-way ANOVA followed by Tukey's *post hoc* test; clear, GCL: $F(1, 44) = 0.1$; ACL: $F(1, 44) = 8.7$; dark, GCL: $F(1, 44) = 0.3$; ACL: $F(1, 44) = 14.3$].(For interpretation of the references to color in this figure legend, the reader is referred to the web version of this article.)

lipoproteins (Feltes et al., 2020) and lysosomal exocytosis depending on calcium (Chen et al., 2010) and mucolipin-1 (Vacca et al., 2019). Our observations in serum-free primary cultures of purified RGCs suggested that CD enables neurons to release lipid-laden lamellar inclusions into the extracellular space (Demais et al., 2016). Our new findings provide evidence that this process occurs *in vivo*. The appearance of extravasate neutrophils and the presence of lamellar inclusions in retinal glial cells upon CD injection in mutant mice suggest that these structures were released by neurons and thereby triggered responses from non-neuronal cells. Why should neurons secrete these structures? This mode is probably the only way for these highly specialized cells to prevent lipid overload. Defects in NPC1 or NPC2 protein enhance the intracellular pool of cholesterol in patient fibroblasts by ten-fold (Lange et al., 1998), and a similarly sized lipid burden can be expected in NPC1-deficient neurons. Neurons are probably unable to handle this large amount of lipids as they cannot esterify and store cholesterol (Aqul et al., 2011; Nieweg et al., 2009; Peake and Vance, 2012; Saadane et al., 2019; Zheng et al., 2012). Moreover, their unique pathway to eliminate surplus cholesterol by CYP46A1-mediated conversion to 24S-hydroxycholesterol may become saturated (Lund et al., 1999; Lutjohann et al., 1996; Pfrieger and Ungerer, 2011). In the retina, this enzyme is expressed by RGCs (Bretillon et al., 2007; Nieweg et al., 2009; Pikuleva and Curcio, 2014; Zheng et al., 2012). These assumptions are supported by findings that intra-cerebroventricular injection of CD in NPC1-deficient mice did not affect cholesteryl ester synthesis or Cyp46a1 expression in the brain (Aqul et al., 2011). The CD-induced enhancement of 24S-hydroxycholesterol levels in the cerebrospinal fluid of NPC disease patients was probably due to decreased loss of neurons (Ory et al., 2017).

Our observation that CD administration induced strongly enlarged phagosomes filled with lamellar inclusions in glial cells suggests that these cells handle the superfluous material released from neurons. Glial cells are activated in the CNS of NPC disease patients and animal models with distinct cell type- and region-specific onsets (Baudry et al., 2003; Cologna et al., 2014; Cougnoux et al., 2018; Cougnoux et al., 2020; Gabande-Rodriguez et al., 2019; German et al., 2002; Kavetsky et al., 2019; Lopez et al., 2011; Luan et al., 2008; Maue et al., 2012; Maulik et al., 2012; Park et al., 2019; Pressey et al., 2012; Repa et al., 2007; Santiago-Mujica et al., 2019; Seo et al., 2014; Stein et al., 2012; Tanaka et al., 1988; Walterfang et al., 2020; Yan et al., 2014a; Yan et al., 2014b). Several studies reported that CD attentuates glial activation (Aqul et al., 2011; Cougnoux et al., 2018; Liu et al., 2009; Maulik et al., 2012; Meyer et al., 2018; Park et al., 2019; Ramirez et al., 2010), but these observations were made weeks after drug injections. We suggest that astrocytes and microglial cells bearing clear and dark cytoplasm take up inclusions, respectively. These cells are known to clear debris and surplus lipids from the healthy and diseased brain (Chausse et al., 2020; Galloway et al., 2019; Loving and Bruce, 2020; Márquez-Ropero et al., 2020; Prinz et al., 2019; Tremblay et al., 2019; Yang et al., 2021). Recent studies suggested that phagocytotic activity of microglial cells is affected by NPC1 deficiency *in vivo* (Boyle et al., 2020; Colombo et al., 2021; Kavetsky et al., 2019) and *in vitro* (Peake et al., 2011; Stein et al., 2012), but these changes are probably overcome by CD (Colombo et al., 2021; Peake and Vance, 2012). Notably, Müller cells, which can be readily identified by their location and ultrastructural features, seemed largely unaffected by NPC1 deficiency at the presymptomatic age and they showed no discernable ultrastructural changes in response to CD injection. This observation underlines the exquisite specialisation of glial cells in the retina (Vecino et al., 2016).

Taken together, our data suggest that the CD-induced reversal of cholesterol accumulation in NPC1-deficient retinal neurons is a non-cell autonomous process requiring coordinated interactions with glial cells. Future studies should analyse the immediate cellular reactions to CD and other therapeutics in brain areas most affected by the disease and explore glial cells as drug targets allowing to optimize the outcome of therapeutic approaches for NPC disease.

Funding

This work was supported by Centre National de la Recherche Scientifique (FWP; contract UPR3212) and the University of Strasbourg (FWP), and project-based funding from Niemann-Pick Selbsthilfegruppe e.V. (FWP), Fondation pour la Recherche Médicale (FWP; Dossier FRM ING20160435315), the association Vaincre les Maladies Lysosomales (FWP) and an EMBO short term fellowship (TH; contract number 8218).

Declarations of interest

None.

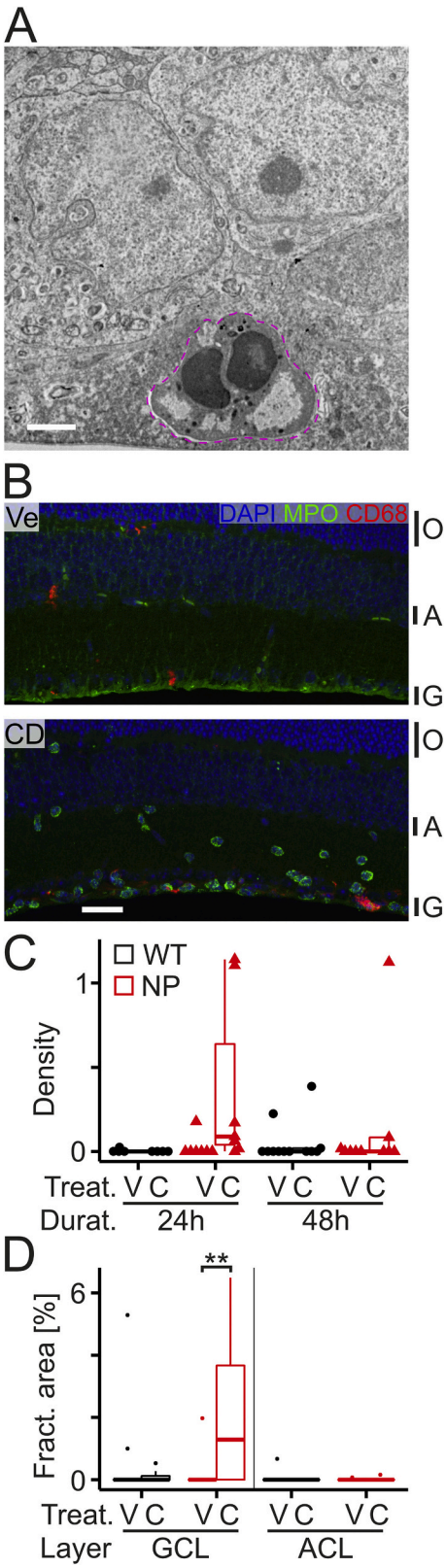

(caption on next column)

Fig. 7. CD-induced presence of neutrophil granulocytes in retinae of NPC1-deficient mice.

A, Electron micrograph showing a cell in the nerve fiber layer (outlined in magenta) with typical ultrastructural features of neutrophil granulocytes. Retinal section from a NPC1-deficient (NP) mouse 48 h after intravitreal injection of 2-hydroxypropyl-beta-cyclodextrin (CD). Scale bar: 2 μm. B, False-color fluorescence micrographs showing the distribution of MPO-positive granulocytes (green), CD68-positive microglia (red) and of DAPI-positive nuclei (blue) in retinal sections from NP mice after intravitreal injection of vehicle (Ve) and CD. Scale bar: 50 μm. For orientation, selected retinal layers are indicated: O, outer nuclear layer; A, amacrine cell layer; G, ganglion cell layer. C, Plots showing boxplots and individual densities of MPO-positive/CD68-negative cells per 10,000 square pixels in retinal sections from wild-type (WT) and NP mice at indicated times after intravitreal injections of vehicle (V) or CD (C). The CD-induced increase in the density in NP mice did not reach statistical significance [$p > 0.05$, three-way ANOVA $F(1, 36) = 0.2$; 24 h, WT Vehicle/CD: $n = 4/4$ animals, NP V/CD: 7/7; 48 h, WT V/CD: 7/5, NP V/CD: 5/5]. D, Boxplots showing the fractional area occupied by neutrophil-like cells in the retinal ganglion cell layer (GCL) and amacrine cell layer (ACL) from WT and NP animals at 24 or 48 h after intravitreal injections of vehicle (V) or CD (C) in the left and right eye, respectively (WT Vehicle/CD: $n = 10/10$ animals; NP V/C: 17/16). CD increased the fractional area covered by neutrophil granulocytes in NP mice (three-way ANOVA followed by Tukey's *post hoc* test; $F(1, 48) = 9.3$).(For interpretation of the references to color in this figure legend, the reader is referred to the web version of this article.)

Acknowledgements

We thank Yvonnick Pongérard and Nolwenn Couqueberg for help with the management of the mouse colony.

References

Abi-Mosleh, L., et al., 2009. Cyclodextrin overcomes deficient lysosome-to-endoplasmic reticulum transport of cholesterol in Niemann-Pick type C cells. Proc. Natl. Acad. Sci. U. S. A. 106, 19316–19321. https://doi.org/10.1073/pnas.0910916106.

Anzil, A.P., et al., 1973. Niemann-Pick disease type-C - case report with ultrastructural findings. Neuropadiatrie. 4, 207–225. https://doi.org/10.1055/s-0028-1091741.

Aqul, A., et al., 2011. Unesterified cholesterol accumulation in late endosomes/lysosomes causes neurodegeneration and is prevented by driving cholesterol export from this compartment. J. Neurosci. 31, 9404–9413. https://doi.org/10.1523/JNEUROSCI.1317-11.2011.

Argüello, G., Balboa, E., Tapia, P.J., Castro, J., Yañez, M.J., Mattar, P., Pulgar, R., Zanlungo, S., 2021. Genistein activates transcription factor EB and corrects Niemann-Pick C phenotype. Int. J. Mol. Sci. 22 (8), 4220. https://doi.org/10.3390/ijms22084220.

Banks, W.A., et al., 2019. Modest blood-brain barrier permeability of the cyclodextrin kleptose: modification by efflux and luminal surface binding. J. Pharmacol. Exp. Ther. 371, 121–129. https://doi.org/10.1124/jpet.119.260497.

Baudry, M., et al., 2003. Postnatal development of inflammation in a murine model of Niemann-Pick type C disease: immunohistochemical observations of microglia and astroglia. Exp. Neurol. 184, 887–903. https://doi.org/10.1016/s0014-4886(03)00345-5.

Berry-Kravis, E., et al., 2018. Long-term treatment of Niemann-Pick type C1 disease with intrathecal 2-hydroxypropyl-β-cyclodextrin. Pediatr. Neurol. 80, 24–34. https://doi.org/10.1016/j.pediatrneurol.2017.12.014.

Bisht, K., et al., 2016. Dark microglia: a new phenotype predominantly associated with pathological states. Glia. 64, 826–839. https://doi.org/10.1002/glia.22966.

Boyle, B.R., et al., 2020. NPC1 deficiency impairs cerebellar postnatal development of microglia and climbing fiber refinement in a mouse mode of Niemann-Pick disease type C. Development. 147 https://doi.org/10.1242/dev.189019.

Bräuer, A.U., et al., 2019. Current challenges in understanding the cellular and molecular mechanisms in Niemann-Pick disease type C1. Int. J. Mol. Sci. 20 https://doi.org/10.3390/ijms20184392.

Breiden, B., Sandhoff, K., 2020. Mechanism of secondary ganglioside and lipid accumulation in lysosomal disease. Int. J. Mol. Sci. 21 https://doi.org/10.3390/ijms21072566.

Bretillon, L., et al., 2007. Cholesterol-24S-hydroxylase (CYP46A1) is specifically expressed in neurons of the neural retina. Curr. Eye Res. 32, 361–366.

Buard, I., Pfrieger, F.W., 2014. Relevance of neuronal and glial NPC1 for synaptic input to cerebellar Purkinje cells. Mol. Cell. Neurosci. 61, 65–71. https://doi.org/10.1016/j.mcn.2014.06.003.

Camargo, F., et al., 2001. Cyclodextrins in the treatment of a mouse model of Niemann-Pick C disease. Life Sci. 70, 131–142. https://doi.org/10.1016/s0024-3205(01)01384-4.

Chausse, B., et al., 2020. Microglia and lipids: how metabolism controls brain innate immunity. Semin. Cell Dev. Biol. 112, 137–144. https://doi.org/10.1016/j.semcdb.2020.08.001.

Chen, Y., et al., 2008. NS21: re-defined and modified supplement B27 for neuronal cultures. J. Neurosci. Methods 171, 239–247. https://doi.org/10.1016/j.jneumeth.2008.03.013.

Chen, F.W., et al., 2010. Cyclodextrin induces calcium-dependent lysosomal exocytosis. PLoS One 5, e15054. https://doi.org/10.1371/journal.pone.0015054.

Clarke, E., Scott-Sherrill-Mix, S., 2017. Categorical Scatter (Violin Point) Plots. https://CRAN.R-project.org/package=ggbeeswarm.

Claudepierre, T., et al., 2010. Lack of Niemann Pick type C1 induces age-related degeneration in the mouse retina. Mol. Cell. Neurosci. 43, 164–176. https://doi.org/10.1016/j.mcn.2009.10.007.

Coisne, C., et al., 2016. Cyclodextrins as emerging therapeutic tools in the treatment of cholesterol-associated vascular and neurodegenerative diseases. Molecules. 21 https://doi.org/10.3390/molecules21121748.

Cologna, S.M., et al., 2014. Human and mouse neuroinflammation markers in Niemann-Pick disease, type C1. J. Inherit. Metab. Dis. 37, 83–92. https://doi.org/10.1007/s10545-013-9610-6.

Colombo, A., et al., 2021. Loss of NPC1 enhances phagocytic uptake and impairs lipid trafficking in microglia. Nat. Commun. 12, 1158. https://doi.org/10.1038/s41467-021-21428-5.

Cougnoux, A., et al., 2018. Microglia activation in Niemann-Pick disease, type C1 is amendable to therapeutic intervention. Hum. Mol. Genet. 27, 2076–2089. https://doi.org/10.1093/hmg/ddy112.

Cougnoux, A., et al., 2020. Single cell transcriptome analysis of Niemann-Pick disease, Type C1 Cerebella. Int. J. Mol. Sci. 21 https://doi.org/10.3390/ijms21155368.

Crini, G., 2014. Review: a history of cyclodextrins. Chem. Rev. 114, 10940–10975. https://doi.org/10.1021/cr500081p.

Cutrone, G., et al., 2017. Cyclodextrin-modified inorganic materials for the construction of nanocarriers. Int. J. Pharm. 531, 621–639. https://doi.org/10.1016/j.ijpharm.2017.06.080.

Dai, S., et al., 2017. Methyl-beta-cyclodextrin restores impaired autophagy flux in Niemann-Pick C1-deficient cells through activation of AMPK. Autophagy. 13, 1435–1451. https://doi.org/10.1080/15548627.2017.1329081.

Davidson, C.D., et al., 2009. Chronic cyclodextrin treatment of murine Niemann-Pick C disease ameliorates neuronal cholesterol and glycosphingolipid storage and disease progression. PLoS One 4, e6951. https://doi.org/10.1371/journal.pone.0006951.

Del Amo, E.M., et al., 2017. Pharmacokinetic aspects of retinal drug delivery. Prog. Retin. Eye Res. 57, 134–185. https://doi.org/10.1016/j.preteyeres.2016.12.001.

Demais, V., et al., 2016. Reversal of pathologic lipid accumulation in NPC1-deficient neurons by drug-promoted release of LAMP1-coated lamellar inclusions. J. Neurosci. 36, 8012–8025. https://doi.org/10.1523/jneurosci.0900-16.2016.

Donida, B., et al., 2020. Nanoparticles containing beta-cyclodextrin potentially useful for the treatment of Niemann-pick C. J. Inherit. Metab. Dis. 43, 586–601. https://doi.org/10.1002/jimd.12210.

Duvvuri, B., et al., 2020. Neutrophil extracellular traps in tissue and periphery in juvenile dermatomyositis. Arthritis Rheum. 72, 348–358. https://doi.org/10.1002/art.41078.

Farmer, C.A., et al., 2019. Long-term neuropsychological outcomes from an open-label phase I/IIa trial of 2-hydroxypropyl-beta-cyclodextrins (VTS-270) in Niemann-Pick disease, type C1. CNS Drugs. 33, 677–683. https://doi.org/10.1007/s40263-019-00642-2.

Feltes, M., et al., 2020. Monitoring the itinerary of lysosomal cholesterol in Niemann-Pick type C1-deficient cells after cyclodextrin treatment. J. Lipid Res. 61, 403–412. https://doi.org/10.1194/jlr.RA119000571.

Fukaura, M., et al., 2021. Intracerebroventricular treatment with 2-hydroxypropyl-β-cyclodextrin decreased cerebellar and hepatic glycoprotein nonmetastatic melanoma protein B (GPNMB) expression in Niemann-Pick disease type C model mice. Int. J. Mol. Sci. 22, 452. https://doi.org/10.3390/ijms22010452.

Gabande-Rodriguez, E., et al., 2019. Lipid-induced lysosomal damage after demyelination corrupts microglia protective function in lysosomal storage disorders. EMBO J. 38, e99553. https://doi.org/10.15252/embj.201899553.

Galloway, D.A., et al., 2019. Phagocytosis in the brain: homeostasis and disease. Front. Immunol. 10, 790. https://doi.org/10.3389/fimmu.2019.00790.

Geberhiwot, T., et al., 2018. Consensus clinical management guidelines for Niemann-Pick disease type C. Orphanet J. Rare Dis. 13, 50. https://doi.org/10.1186/s13023-018-0785-7.

German, D.C., et al., 2002. Neurodegeneration in the Niemann-Pick C mouse: glial involvement. Neuroscience. 109, 437–450. https://doi.org/10.1016/S0306-4522(01)00517-6.

Gowrishankar, S., et al., 2020. Deregulation of signalling in genetic conditions affecting the lysosomal metabolism of cholesterol and galactosyl-sphingolipids. Neurobiol. Dis. 146, 105142. https://doi.org/10.1016/j.nbd.2020.105142.

Griffin, L.D., et al., 2004. Niemann-Pick type C disease involves disrupted neurosteroidogenesis and responds to allopregnanolone. Nat. Med. 10, 704–711. https://doi.org/10.1038/nm1073.

Hammond, N., et al., 2019. The complexity of a monogenic neurodegenerative disease: more than two decades of therapeutic driven research into Niemann-Pick type C disease. Biochim. Biophys. Acta Mol. Cell Biol. Lipids 1864, 1109–1123. https://doi.org/10.1016/j.bbalip.2019.04.002.

Harzer, K., et al., 1978. Neurovisceral lipidosis compatible with Niemann-Pick disease type C: morphological and biochemical studies of a late infantile case and enzyme and lipid assays in a prenatal case of the same family. Acta Neuropathol. 43, 97–104.

Havla, J., et al., 2020. Retinal axonal degeneration in Niemann-Pick type C disease. J. Neurol. 267, 2070–2082. https://doi.org/10.1007/s00415-020-09796-2.

Heybrock, S., et al., 2019. Lysosomal integral membrane protein-2 (LIMP-2/SCARB2) is involved in lysosomal cholesterol export. Nat. Commun. 10, 3521. https://doi.org/10.1038/s41467-019-11425-0.

Karten, B., et al., 2002. Cholesterol accumulates in cell bodies, but is decreased in distal axons, of Niemann-Pick C1-deficient neurons. J. Neurochem. 83, 1154–1163. https://doi.org/10.1046/j.1471-4159.2002.01220.x.

Kavetsky, L., et al., 2019. Increased interactions and engulfment of dendrites by microglia precede Purkinje cell degeneration in a mouse model of Niemann Pick type-C. Sci. Rep. 9, 14722. https://doi.org/10.1038/s41598-019-51246-1.

Kobayashi, T., et al., 1999. Late endosomal membranes rich in lysobisphosphatidic acid regulate cholesterol transport. Nat. Cell Biol. 1, 113–118. https://doi.org/10.1038/10084.

Kurkov, S.V., Loftsson, T., 2013. Cyclodextrins. Int. J. Pharm. 453, 167–180. https://doi.org/10.1016/j.ijpharm.2012.06.055.

Kwiatkowska, K., et al., 2014. Visualization of cholesterol deposits in lysosomes of Niemann-Pick type C fibroblasts using recombinant perfringolysin O. Orphanet J. Rare Dis. 9, 64. https://doi.org/10.1186/1750-1172-9-64.

Kwon, H.J., et al., 2009. Structure of N-terminal domain of NPC1 reveals distinct subdomains for binding and transfer of cholesterol. Cell. 137, 1213–1224. https://doi.org/10.1016/j.cell.2009.03.049.

Lange, Y., et al., 1998. Circulation of cholesterol between lysosomes and the plasma membrane. J. Biol. Chem. 273, 18915–18922. https://doi.org/10.1074/jbc.273.30.18915.

Li, X., et al., 2017. 3.3 Å structure of Niemann-Pick C1 protein reveals insights into the function of the C-terminal luminal domain in cholesterol transport. Proc. Natl. Acad. Sci. U. S. A. 114, 9116–9121. https://doi.org/10.1073/pnas.1711716114.

Liscum, L., Faust, J.R., 1989. The intracellular transport of low density lipoprotein-derived cholesterol is inhibited in Chinese hamster ovary cells cultured with 3-beta-[2-(diethylamino)ethoxy]androst-5-en-17-one. J. Biol. Chem. 264, 11796–11806. https://doi.org/10.1016/S0021-9258(18)80136-3.

Liscum, L., et al., 1989. The intracellular transport of low density lipoprotein-derived cholesterol is defective in Niemann-Pick type C fibroblasts. J. Cell Biol. 108, 1625–1636. https://doi.org/10.1083/jcb.108.5.1625.

Liu, Y., et al., 2003. Control of the size and distribution of gold nanoparticles by unmodified cyclodextrins. Chem. Mater. 15, 4172–4180. https://doi.org/10.1021/cm0342041.

Liu, B., et al., 2008. Genetic variations and treatments that affect the lifespan of the NPC1 mouse. J. Lipid Res. 49, 663–669. https://doi.org/10.1194/jlr.m700525-jlr200.

Liu, B., et al., 2009. Reversal of defective lysosomal transport in NPC disease ameliorates liver dysfunction and neurodegeneration in the npc1−/− mouse. Proc. Natl. Acad. Sci. U. S. A. 106, 2377–2382. https://doi.org/10.1073/pnas.0810895106.

Lloyd-Evans, E., et al., 2008. Niemann-Pick disease type C1 is a sphingosine storage disease that causes deregulation of lysosomal calcium. Nat. Med. 14, 1247–1255. https://doi.org/10.1038/nm.1876.

Loftus, S.K., et al., 1997. Murine model of Niemann-Pick C disease: mutation in a cholesterol homeostasis gene. Science. 277, 232–235. https://doi.org/10.1126/science.277.5323.232.

Lopez, M.E., et al., 2011. Anatomically defined neuron-based rescue of neurodegenerative Niemann-Pick type C disorder. J. Neurosci. 31, 4367–4378. https://doi.org/10.1523/jneurosci.5981-10.2011.

Love, S., et al., 1995. Neurofibrillary tangles in Niemann-Pick disease type C. Brain. 118, 119–129. https://doi.org/10.1093/brain/118.1.119.

Loving, B.A., Bruce, K.D., 2020. Lipid and lipoprotein metabolism in microglia. Front. Physiol. 11, 393. https://doi.org/10.3389/fphys.2020.00393.

Lowenthal, A.C., et al., 1990. Feline sphingolipidosis resembling Niemann-Pick disease type C. Acta Neuropathol. 81, 189–197. https://doi.org/10.1007/BF00334507.

Lu, F., et al., 2015. Identification of NPC1 as the target of U18666A, an inhibitor of lysosomal cholesterol export and Ebola infection. Elife 4, e12177. https://doi.org/10.7554/elife.12177.

Luan, Z., et al., 2008. Brainstem neuropathology in a mouse model of Niemann-Pick disease type C. J. Neurol. Sci. 268, 108–116. https://doi.org/10.1016/j.jns.2007.11.018.

Lund, E.G., et al., 1999. cDNA cloning of cholesterol 24-hydroxylase, a mediator of cholesterol homeostasis in the brain. Proc. Natl. Acad. Sci. U. S. A. 96, 7238–7243. https://doi.org/10.1073/pnas.96.13.7238.

Lutjohann, D., et al., 1996. Cholesterol homeostasis in human brain: evidence for an age-dependent flux of 24S-hydroxycholesterol from the brain into the circulation. Proc. Natl. Acad. Sci. U. S. A. 93, 9799–9804. https://doi.org/10.1073/pnas.93.18.9799.

Márquez-Ropero, M., et al., 2020. Microglial corpse clearance: lessons from macrophages. Front. Immunol. 11, 506. https://doi.org/10.3389/fimmu.2020.00506.

Masse, F., et al., 2019. Gold nanoparticles in ophthalmology. Med. Res. Rev. 39, 302–327. https://doi.org/10.1002/med.21509.

Maue, R.A., et al., 2012. A novel mouse model of Niemann-Pick type C disease carrying a D1005G-Npc1 mutation comparable to commonly observed human mutations. Hum. Mol. Genet. 21, 730–750. https://doi.org/10.1093/hmg/ddr505.

Maulik, M., et al., 2012. Mutant human APP exacerbates pathology in a mouse model of NPC and its reversal by a beta-cyclodextrin. Hum. Mol. Genet. 21, 4857–4875. https://doi.org/10.1093/hmg/dds322.

Meske, V., et al., 2014. The autophagic defect in Niemann-Pick disease type C neurons differs from somatic cells and reduces neuronal viability. Neurobiol. Dis. 64, 88–97. https://doi.org/10.1016/j.nbd.2013.12.018.

Meyer, A., et al., 2018. Olfactory performance as an indicator for protective treatment effects in an animal model of neurodegeneration. Front. Integr. Neurosci. 12, 35. https://doi.org/10.3389/fnint.2018.00035.

Monnaert, V., et al., 2004. Behavior of α-, β-, and γ-cyclodextrins and their derivatives on an in vitro model of blood-brain barrier. J. Pharmacol. Exp. Ther. 310, 745–751. https://doi.org/10.1124/jpet.104.067512.
Naureckiene, S., et al., 2000. Identification of HE1 as the second gene of Niemann-Pick C disease. Science. 290, 2298–2301. https://doi.org/10.1126/science.290.5500.2298.
Nieweg, K., et al., 2009. Marked differences in cholesterol synthesis between neurons and glial cells from postnatal rats. J. Neurochem. 109, 125–134. https://doi.org/10.1111/j.1471-4159.2009.05917.x.
Norman, A.W., et al., 1972. Studies on the biological properties of polyene antibiotics. Evidence for the direct interaction of filipin with cholesterol. J. Biol. Chem. 247, 1918–1929. https://doi.org/10.1016/S0021-9258(19)45558-0.
Ory, D.S., et al., 2017. Intrathecal 2-hydroxypropyl-β-cyclodextrin decreases neurological disease progression in Niemann-Pick disease, type C1: a non-randomised, open-label, phase 1-2 trial. Lancet. 390, 1758–1768. https://doi.org/10.1016/s0140-6736(17)31465-4.
Palladino, G., et al., 2015. Visual evoked potentials of Niemann-Pick type C1 mice reveal an impairment of the visual pathway that is rescued by 2-hydroxypropyl-ß-cyclodextrin. Orphanet J. Rare Dis. 10, 133. https://doi.org/10.1186/s13023-015-0348-0.
Pallottini, V., Pfrieger, F.W., 2020. Understanding and treating Niemann-Pick type C disease: models matter. Int. J. Mol. Sci. 21, 8979. https://doi.org/10.3390/ijms21238979.
Palmer, M., et al., 1985. Niemann-pick disease–type C. Ocular histopathologic and electron microscopic studies. Arch. Ophthalmol. 103, 817–822. https://doi.org/10.1001/archopht.1985.01050060077030.
Park, M.H., et al., 2019. Characterization of the subventricular-thalamo-cortical circuit in the NP-C mouse brain, and new insights regarding treatment. Mol. Ther. 27, 1507–1526. https://doi.org/10.1016/j.ymthe.2019.05.008.
Peake, K.B., Vance, J.E., 2012. Normalization of cholesterol homeostasis by 2-hydroxypropyl-beta-cyclodextrin in neurons and glia from Niemann-Pick C1 (NPC1)-deficient mice. J. Biol. Chem. 287, 9290–9298. https://doi.org/10.1074/jbc.m111.326405.
Peake, K.B., et al., 2011. Niemann-Pick type C1 deficiency in microglia does not cause neuron death in vitro. Biochim. Biophys. Acta 1812, 1121–1129. https://doi.org/10.1016/j.bbadis.2011.06.003.
Pentchev, P.G., et al., 1985. A defect in cholesterol esterification in Niemann-Pick disease (type C) patients. Proc. Natl. Acad. Sci. U. S. A. 82, 8247–8251. https://doi.org/10.1073/pnas.82.23.8247.
Peters, A., et al., 1991. The Fine Structure of the Nervous System: The Neurons and Supporting Cells. Oxford University Press, Oxford.
Pfeffer, S.R., 2019. NPC intracellular cholesterol transporter 1 (NPC1)-mediated cholesterol export from lysosomes. J. Biol. Chem. 294, 1706–1709. https://doi.org/10.1074/jbc.TM118.004165.
Pfrieger, F.W., Ungerer, N., 2011. Cholesterol metabolism in neurons and astrocytes. Prog. Lipid Res. 50, 357–371. https://doi.org/10.1016/j.plipres.2011.06.002.
Phillips, S.E., et al., 2008. Neuronal loss of Drosophila NPC1a causes cholesterol aggregation and age-progressive neurodegeneration. J. Neurosci. 28, 6569–6582. https://doi.org/10.1523/jneurosci.5529-07.2008.
Pikuleva, I.A., Curcio, C.A., 2014. Cholesterol in the retina: the best is yet to come. Prog. Retin. Eye Res. 41, 64–89. https://doi.org/10.1016/j.preteyeres.2014.03.002.
Plazzo, A.P., et al., 2012. Uptake of a fluorescent methyl-β-cyclodextrin via clathrin-dependent endocytosis. Chem. Phys. Lipids 165, 505–511. https://doi.org/10.1016/j.chemphyslip.2012.03.007.
Pontikis, C.C., et al., 2013. Cyclodextrin alleviates neuronal storage of cholesterol in Niemann-Pick C disease without evidence of detectable blood-brain barrier permeability. J. Inherit. Metab. Dis. 36, 491–498. https://doi.org/10.1007/s10545-012-9583-x.
Praggastis, M., et al., 2015. A murine Niemann-Pick C1 I1061T knock-in model recapitulates the pathological features of the most prevalent human disease allele. J. Neurosci. 35, 8091–8106. https://doi.org/10.1523/jneurosci.4173-14.2015.
Pressey, S.N., et al., 2012. Early glial activation, synaptic changes and axonal pathology in the thalamocortical system of Niemann-Pick type C1 mice. Neurobiol. Dis. 45, 1086–1100. https://doi.org/10.1016/j.nbd.2011.12.027.
Prinz, M., et al., 2019. Microglia biology: one century of evolving concepts. Cell. 179, 292–311. https://doi.org/10.1016/j.cell.2019.08.053.
Qian, H., et al., 2020. Structural basis of low-pH-dependent lysosomal cholesterol egress by NPC1 and NPC2. Cell 182, 98–111.e18. https://doi.org/10.1016/j.cell.2020.05.020.
R Core Team, 2021. R: A Language and Environment for Statistical Computing. R Foundation for Statistical Computing, Vienna, Austria. https://www.R-project.org/.
Ramírez, J.M., et al., 1996. Structural specializations of human retinal glial cells. Vis. Res. 36, 2029–2036. https://doi.org/10.1016/0042-6989(95)00322-3.
Ramirez, C.M., et al., 2010. Weekly cyclodextrin administration normalizes cholesterol metabolism in nearly every organ of the Niemann-Pick type C1 mouse and markedly prolongs life. Pediatr.Res. 68, 309–315. https://doi.org/10.1203/pdr.0b013e3181ee4dd2.
Reid, P.C., et al., 2004. A novel cholesterol stain reveals early neuronal cholesterol accumulation in the Niemann-Pick type C1 mouse brain. J. Lipid Res. 45, 582–591. https://doi.org/10.1194/jlr.d300032-jlr200.
Repa, J.J., et al., 2007. Liver X receptor activation enhances cholesterol loss from the brain, decreases neuroinflammation, and increases survival of the NPC1 mouse. J. Neurosci. 27, 14470–14480. https://doi.org/10.1523/jneurosci.4823-07.2007.
Rosenbaum, A.I., et al., 2010. Endocytosis of beta-cyclodextrins is responsible for cholesterol reduction in Niemann-Pick type C mutant cells. Proc. Natl. Acad. Sci. U. S. A. 107, 5477–5482. https://doi.org/10.1073/pnas.0914309107.
Saadane, A., et al., 2019. Retinal vascular abnormalities and microglia activation in mice with deficiency in cytochrome P450 46A1-mediated cholesterol removal. Am. J. Pathol. 189, 405–425. https://doi.org/10.1016/j.ajpath.2018.10.013.
Santiago-Mujica, E., et al., 2019. Hepatic and neuronal phenotype of NPC1(−/−) mice. Heliyon. 5, e01293 https://doi.org/10.1016/j.heliyon.2019.e01293.
Schmitt, M., et al., 2019. Intravitreal pharmacokinetics in mice: SPECT/CT imaging and scaling to rabbits and humans. Mol. Pharm. 16, 4399–4404. https://doi.org/10.1021/acs.molpharmaceut.9b00679.
Segatto, M., et al., 2014. Simvastatin treatment highlights a new role for the isoprenoid/cholesterol biosynthetic pathway in the modulation of emotional reactivity and cognitive performance in rats. Neuropsychopharmacology 39, 841–854. https://doi.org/10.1038/npp.2013.284.
Seo, Y., et al., 2014. Excessive microglial activation aggravates olfactory dysfunction by impeding the survival of newborn neurons in the olfactory bulb of Niemann-Pick disease type C1 mice. Biochim. Biophys. Acta 1842, 2193–2203. https://doi.org/10.1016/j.bbadis.2014.08.005.
Sokol, J., et al., 1988. Type C Niemann-pick disease. Lysosomal accumulation and defective intracellular mobilization of low density lipoprotein cholesterol. J. Biol. Chem. 263, 3411–3417. https://doi.org/10.1016/S0021-9258(18)69086-6.
Stein, V.M., et al., 2012. Miglustat improves purkinje cell survival and alters microglial phenotype in feline niemann-pick disease type C. J. Neuropathol. Exp. Neurol. 71, 434–448. https://doi.org/10.1097/nen.0b013e31825414a6.
Tanaka, J., et al., 1988. Cerebellar involvement in murine sphingomyelinosis: a new model of Niemann-Pick disease. J. Neuropathol. Exp. Neurol. 47, 291–300. https://doi.org/10.1097/00005072-198805000-00008.
Toledano-Zaragoza, A., Ledesma, M.D., 2020. Addressing neurodegeneration in lysosomal storage disorders: advances in Niemann Pick diseases. Neuropharmacology. 171 https://doi.org/10.1016/j.neuropharm.2019.107851.
Tremblay, M.E., et al., 2019. Glial phagocytic clearance in Parkinson's disease. Mol. Neurodegener. 14, 16. https://doi.org/10.1186/s13024-019-0314-8.
Vacca, F., et al., 2019. Cyclodextrin triggers MCOLN1-dependent endo-lysosome secretion in Niemann-Pick type C cells. J. Lipid Res. 60, 832–843. https://doi.org/10.1194/jlr.M089979.
Vance, J.E., Karten, B., 2014. Niemann-Pick C disease and mobilization of lysosomal cholesterol by cyclodextrin. J. Lipid Res. 55, 1609–1621. https://doi.org/10.1194/jlr.r047837.
Vanier, M.T., 2010. Niemann-Pick disease type C. Orphanet J. Rare Dis. 5, 16. https://doi.org/10.1186/1750-1172-5-16.
Vanier, M.T., Latour, P., 2015. Laboratory diagnosis of Niemann-Pick disease type C: the filipin staining test. Methods Cell Biol. 126, 357–375. https://doi.org/10.1016/bs.mcb.2014.10.028.
Varadi, J., et al., 2019. Pharmacokinetic properties of fluorescently labelled hydroxypropyl-beta-cyclodextrin. Biomolecules. 9, 509. https://doi.org/10.3390/biom9100509.
Vecino, E., et al., 2016. Glia-neuron interactions in the mammalian retina. Prog. Retin. Eye Res. 51, 1–40. https://doi.org/10.1016/j.preteyeres.2015.06.003.
Vite, C.H., et al., 2015. Intracisternal cyclodextrin prevents cerebellar dysfunction and Purkinje cell death in feline Niemann-Pick type C1 disease. Sci. Transl. Med. 7, 276ra26. https://doi.org/10.1126/scitranslmed.3010101.
Walterfang, M., et al., 2020. Imaging of neuroinflammation in adult Niemann-Pick type C disease: a cross-sectional study. Neurology. 94, e1716–e1725. https://doi.org/10.1212/wnl.0000000000009287.
Wheeler, S., Sillence, D.J., 2020. Niemann-Pick type C disease: cellular pathology and pharmacotherapy. J. Neurochem. 153, 674–692. https://doi.org/10.1111/jnc.14895.
Wickham, H., 2016. ggplot2: Elegant Graphics for Data Analysis. Springer-Verlag New York.
Winkler, M.B.L., et al., 2019. Structural insight into eukaryotic sterol transport through Niemann-Pick type C proteins. Cell 179, 485–497.e18. https://doi.org/10.1016/j.cell.2019.08.038.
Yan, X., et al., 2014a. Defects in the retina of Niemann-pick type C 1 mutant mice. BMC Neurosci. 15, 126. https://doi.org/10.1186/s12868-014-0126-2.
Yan, X., et al., 2014b. Hyperactive glial cells contribute to axonal pathologies in the spinal cord of Npc1 mutant mice. Glia. 62, 1024–1040. https://doi.org/10.1002/glia.22659.
Yang, S., et al., 2021. Microglia reprogram metabolic profiles for phenotype and function changes in central nervous system. Neurobiol. Dis. 152, 105290. https://doi.org/10.1016/j.nbd.2021.105290.
Yipp, B.G., et al., 2012. Infection-induced NETosis is a dynamic process involving neutrophil multitasking in vivo. Nat. Med. 18, 1386–1393. https://doi.org/10.1038/nm.2847.
Zervas, M., et al., 2001. Neurons in Niemann-Pick disease type C accumulate gangliosides as well as unesterified cholesterol and undergo dendritic and axonal alterations. J. Neuropathol. Exp. Neurol. 60, 49–64. https://doi.org/10.1093/jnen/60.1.49.
Zheng, W., et al., 2012. Spatial distribution of the pathways of cholesterol homeostasis in human retina. PLoS One 7, e37926. https://doi.org/10.1371/journal.pone.0037926.